The mechanism underlying toxicity of a venom peptide against insects reveals how ants are master at disrupting membranes

Steven Ascoët, Axel Touchard, Nathan Téné, Benjamin Lefranc, Jérôme Leprince, Françoise Paquet, Laurence Jouvensal, Valentine Barassé, Michel Treilhou, Arnaud Billet, et al.

iScience

CellPress
OPEN ACCESS

Article

The mechanism underlying toxicity of a venom peptide against insects reveals how ants are master at disrupting membranes

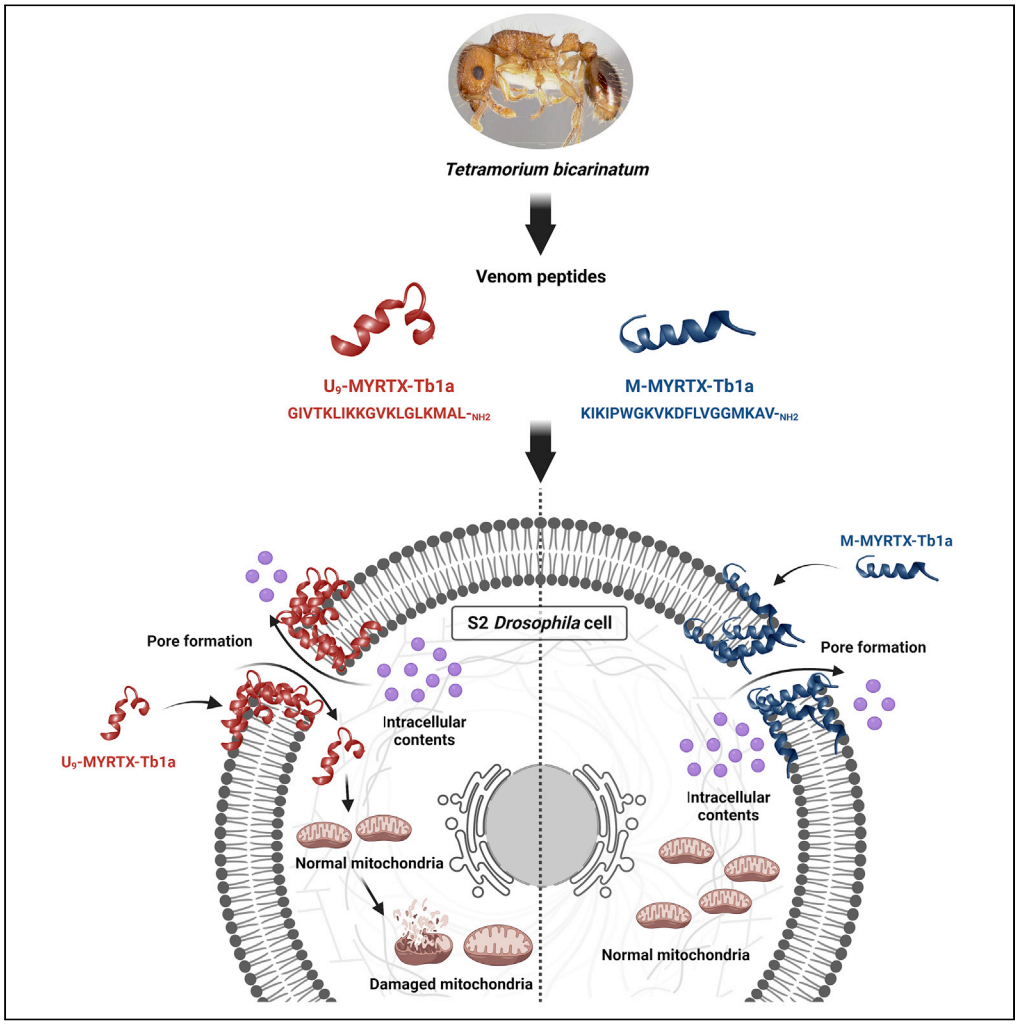

Steven Ascoët, Axel Touchard, Nathan Téné, ..., Michel Treilhou, Arnaud Billet, Elsa Bonnafé

elsa.bonnafe@univ-jfc.fr

Highlights

U_9 has a significant insecticidal activity and induces a cell swelling phenotype

U_9 impacts both metabolism and membrane integrity of cells

U_9 causes cell permeabilization through the formation of pores

U_9 enters into cells and induces a mitochondria disorganization phenotype

Ascoët et al., iScience 26, 106157
March 17, 2023 © 2023
https://doi.org/10.1016/j.isci.2023.106157

iScience

CellPress
OPEN ACCESS

Article

The mechanism underlying toxicity of a venom peptide against insects reveals how ants are master at disrupting membranes

Steven Ascoët,[1] Axel Touchard,[2] Nathan Téné,[1] Benjamin Lefranc,[3,4] Jérôme Leprince,[3,4] Françoise Paquet,[5] Laurence Jouvensal,[5] Valentine Barassé,[1] Michel Treilhou,[1] Arnaud Billet,[1] and Elsa Bonnafé[1,6,*]

SUMMARY

Hymenopterans represent one of the most abundant groups of venomous organisms but remain little explored due to the difficult access to their venom. The development of proteo-transcriptomic allowed us to explore diversity of their toxins offering interesting perspectives to identify new biological active peptides. This study focuses on U_9 function, a linear, amphiphilic and polycationic peptide isolated from ant *Tetramorium bicarinatum* venom. It shares physicochemical properties with M-Tb1a, exhibiting cytotoxic effects through membrane permeabilization. In the present study, we conducted a comparative functional investigation of U_9 and M-Tb1a and explored the mechanisms underlying their cytotoxicity against insect cells. After showing that both peptides induced the formation of pores in cell membrane, we demonstrated that U_9 induced mitochondrial damage and, at high concentrations, localized into cells and induced caspase activation. This functional investigation highlighted an original mechanism of U_9 questioning on potential valorization and endogen activity in *T. bicarinatum* venom.

INTRODUCTION

Venoms are a rich source of valuable bioactive molecules as demonstrated by several venom-derived drugs and one commercialized bioinsecticide.[1–5] Currently, 16 food drug administration approved drugs or therapies are on the market and 21 additional molecules are in clinical trials. All these molecules are derived from the emblematic venomous animals (e.g. snake, spider, cone snail, scorpion)[1,3,4] whereas there is no insect-venom compound in any drug or insecticide development program.

Insects dominate all terrestrial environments and are the most abundant and diverse group of venomous organisms. Despite the clear potential that venomous insects represent, their investigations and characterization remain highly underexplored.[6,7] The main reason for the lack of research on these species is that most are small and provide little venomous material which has made the identification of venom toxins daunting.[1,8,9] Using integrative proteo-transcriptomic methodologies, recent studies have begun to reveal the molecular diversity of flies, true bugs, caterpillars, and Hymenoptera venoms, yielding a large number of novel peptide sequences. The scientific challenge thus shifts from peptide sequencing to the identification of biological activities and the elucidation of pharmacological mechanisms of a vast library of new bioactive toxins.[2,8] To discover promising new peptides and expand the pharmacological profile of insect venoms in terms of novel activities and modes of action, remarkable functional studies on isolated peptides are still needed.

Proteo-transcriptomic investigations conducted on a panel of Hymenoptera now allow us to appreciate the full complexity of venoms and will accelerate the delineation of the biological activity of venom peptides. In particular, the analysis of ant, wasp, or velvet ant venoms, coupled with functional assays, has already identified several new insecticidal,[10–17] antimicrobial,[10,11,18–22] anthelminthic[15,23,24] and pain-causing[10,25–27] peptides. These studies led to the description of the hyperdiverse peptide gene superfamily, called aculeatoxins, which appears to be widespread in Hymenoptera particularly in ant venoms.[10] The aculeatoxins genes encode a wide range of linear amphiphilic and polycationic peptides, most of which have the ability to interact with cell membranes, thus fulfilling multifunctional roles in the venom.[10,27] Of interest, the diversification of aculeatoxins, reflected by the enormous diversity of primary sequences, has also allowed the

[1]BTSB-UR 7417, Université de Toulouse, Institut National Universitaire Jean-François Champollion, Place de Verdun, 81000 Albi, France

[2]CNRS, UMR Ecologie des Forêts de Guyane, AgroParisTech, CIRAD, INRA, Université de Guyane, Université des Antilles, Campus Agronomique, BP316 97310 Kourou, France

[3]Inserm U1239, NorDiC, Laboratoire de Différenciation et Communication Neuroendocrine, Endocrine et Germinale, Université de Rouen-Normandie, 76000 Rouen, France

[4]Inserm US51, HeRacLeS, Université de Rouen-Normandie, 76000 Rouen, France

[5]Centre de Biophysique Moléculaire, CNRS UPR 4301, Rue Charles Sadron CS-80054, 45071 Orléans, France

[6]Lead contact

*Correspondence: elsa.bonnafe@univ-jfc.fr

https://doi.org/10.1016/j.isci.2023.106157

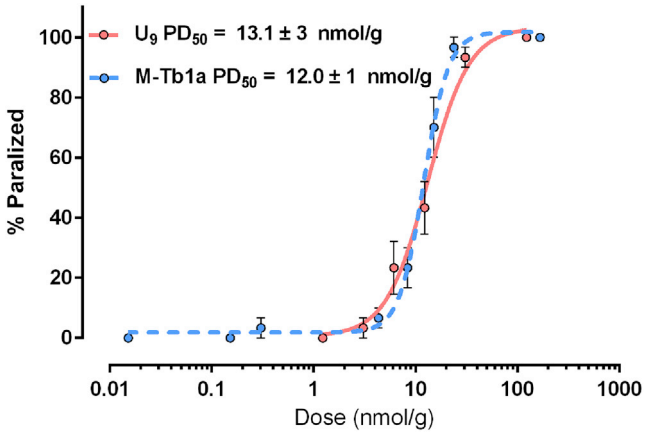

Figure 1. Paralytic activity of M-Tb1a and U_9 against *Lucilia caesar*

The curve was obtained from the injection of M-Tb1a and U_9 into blowflies (*L. caesar*). Percentage was determined 1h after injection. Values are represented as mean ± SEM of three independent experiments.

evolution of specific receptor-modulating peptides such as P17 with mas-related G-protein coupled receptor member X2.[28]

Our research group investigates the venom of the Guinea ant *Tetramorium bicarinatum* whose venom peptidome obtained in our previous study revealed that aculeatoxins are predominant.[29] Among them, we conducted the biological characterization of bicarinalin (named M-Tb1a throughout the paper) and P17, two predominant linear α-helical polycationic peptides. P17 is an immunomodulatory agonist of an orphan G protein-coupled receptor,[28,30] whereas M-Tb1a is a pore-forming peptide displaying antimicrobial effect against a broad spectrum of bacterial strains and cytotoxic activities by membrane permeabilization.[31–35]

To extend the functional characterization of *T. bicarinatum* toxins we focus on another aculeatoxin peptide tentatively named U_9-MYRTX-Tb1a (U9). This peptide shares several features with M-Tb1a including molecular weight, charge, and predicted α-helical secondary structure.[29] This suggests a similar cytotoxic effect to that of M-Tb1a. In the present study, we conducted a comparative functional investigation of U_9 and M-Tb1a and further explored the mechanisms underlying cytotoxicity.

RESULTS

Effect of M-Tb1a and U_9peptides on blowfly

T. bicarinatum uses its venom to capture prey that are mainly small insects and therefore, U_9 and M-Tb1a could participate in the predation function of the venom. Hence, we first investigated the effect of U_9 and M-Tb1a on blowflies by injecting solubilized peptides into the thorax. Both peptides induced a rapid contractile paralysis with similar potency 1h after injection. These results are consistent with the previous study showing that intrathoracic injection of M-Ta1a, a peptide isolated *Tetramorium africanum* venom and similar to M-Tb1a, induced rapid and irreversible paralysis in blowflies (Figure 1). Similarly, most insecticidal venom peptides, which interact with cell membranes, exhibited such effects when injected into insects.[11,26,27]

Cytotoxicity of M-Tb1a and U_9peptides on S2 cells

The lethal and paralytic activity of both peptides observed on blowfly led us to measure the cytotoxic activity of the U_9 and M-Tb1a peptides using *in vitro* assays on the dipteran S2 *Drosophila* embryonic cell line. Both peptides induced cytotoxic effects after 24 h of incubation (Figure 2). For M-Tb1a, similar LC_{50} values were determined with viability (CCK-8) and mortality (LDH) assays: 5.16 and 3.8 μM, respectively (Figure 2A). In contrast, a shift was observed between the two LC_{50} of U_9: 3.15 and 17.97 μM for viability and mortality assays, respectively (Figure 2B). This discrepancy accounts for a cytotoxic effect at a concentration where no cell lysis occurs, called sublytic concentration. Consequently, as shown in Figure 2, the effect of U_9 on cell viability is similar to that of M-Tb1a whereas its cell lysis potential is 6 times lower. Based on these results, the effects of both peptides were examined at the following concentrations: high (50 μM); lytic LC_{50} (M-Tb1a: 4 μM; U_9: 18 μM) and sublytic LC_{50} for U_9 (3.33 μM).

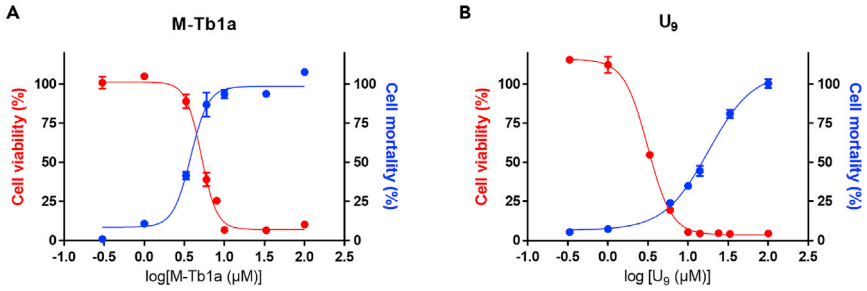

Figure 2. Cytotoxic activities of M-Tb1a and U_9 against *Drosophila* S2 cells

The results were obtained from CCK-8 and LDH assays.

(A) Log(LC_{50}) of M-Tb1a are 0.71 ± 0.02 (5.16 μM) and 0.58 ± 0.03 (3.8 μM) for CCK-8 and LDH assays respectively.

(B) Log(LC_{50}) of U_9 are 0.5 ± 0.01 (3.15 μM) and 1.25 ± 0.04 (17.97 μM) for CCK-8 and LDH assays respectively. The data were normalized from the control according to the manufacturer's recommendations. Values are represented as mean ± SEM (n = 1–8).

Modification of S2 cells morphotypes induced by both peptides

Both peptides induced a cytotoxic activity against cells and could possibly affect the S2 cells morphotypes. We therefore exposed the cells to various concentrations of peptides and monitored their morphologies every 15 min over 1h (Figure 3). The cell morphology was altered with both peptides at all concentrations starting from the first 15 min. M-Tb1a induced progressive cell shrinkage at the lytic LC_{50} (4 μM), and faster at 50 μM (Figure 3). By contrast, U_9 induced cell swelling after 15 min at concentrations of 50 μM and lytic LC_{50} (18 μM), as well as membrane blebs after 30 min of exposure at 50 μM and after 45 min at 18 μM. We observed a few morphological modifications with U_9 at its sublytic LC_{50} (3.33 μM) (Figure 3).

Permeabilization of S2 cells by both peptides

The morphological study showed that both peptides induced opposite morphotypes: (1) swelling for U_9 and (2) shrinkage for M-Tb1a. To understand the observed cellular plasticity, we next studied the permeabilization of S2 cells by using the fluorescent intercalator 7-AminoActinomycin D (7-AAD). At 50 μM, both peptides induced a rapid cell permeabilization (Figure 4B) with a stronger effect for U_9 at 60 min. At lytic LC_{50}, cell permeabilization occurred only with U_9 (Figure 4B) whereas it was not observed at 3.33 μM and 4 μM for U_9 and M-Tb1a respectively (Figure 4B). Furthermore, as shown in Figure 4C, the two peptides induced at the maximal concentration (or lytic LC_{50} for U_9 only) two different permeabilizations (i.e., linear and exponential profiles for M-Tb1a and U_9, respectively), suggesting two different mechanisms for cell permeabilization.

Formation of peptide-induced pores in the cell membrane

The above-mentioned results led us to analyze the structure of S2 cell membranes after exposure to peptides using a scanning electron microscope (SEM). Exposure of cells to M-Tb1a at lytic LC_{50} and U_9 at sublytic LC_{50} resulted in the formation of small pores having a diameter of 50–100 nm (Figure 5). In contrast with M-Tb1a, the lytic concentration of U_9 produced large pores with a size approximately 500–800 nm after 1 h, and larger than 1 μm after 2 h (Figure 5). For the latter, we could describe them as "holes" in the membrane. In addition, at this concentration, the cells displayed smooth surfaces lacking filopodia while exhibiting several vesicle-like elements only observed for this condition. After longer exposure times (8 h and 24 h) at high and lytic concentrations, both peptides induced complete membrane disruption for all cells (Figure S1A). Of note, an expulsion of intracellular contents was observed after 24 h for several cells exposed to U_9 at lytic LC_{50}. (Figure S1B). These data support two distinct mechanisms of action for M-Tb1a and U_9, which lead to the formation of different types of pores.

Mitochondria damages induced by U_9-MYRTX-Tb1a

The results of the CCK-8 viability assays suggest that U_9 may impact cellular metabolism through intracellular effects. For their major role in metabolism, we studied the mitochondria of S2 cells exposed to both peptides by using transmission electron microscopy (TEM). For untreated S2 cells, the mitochondria are

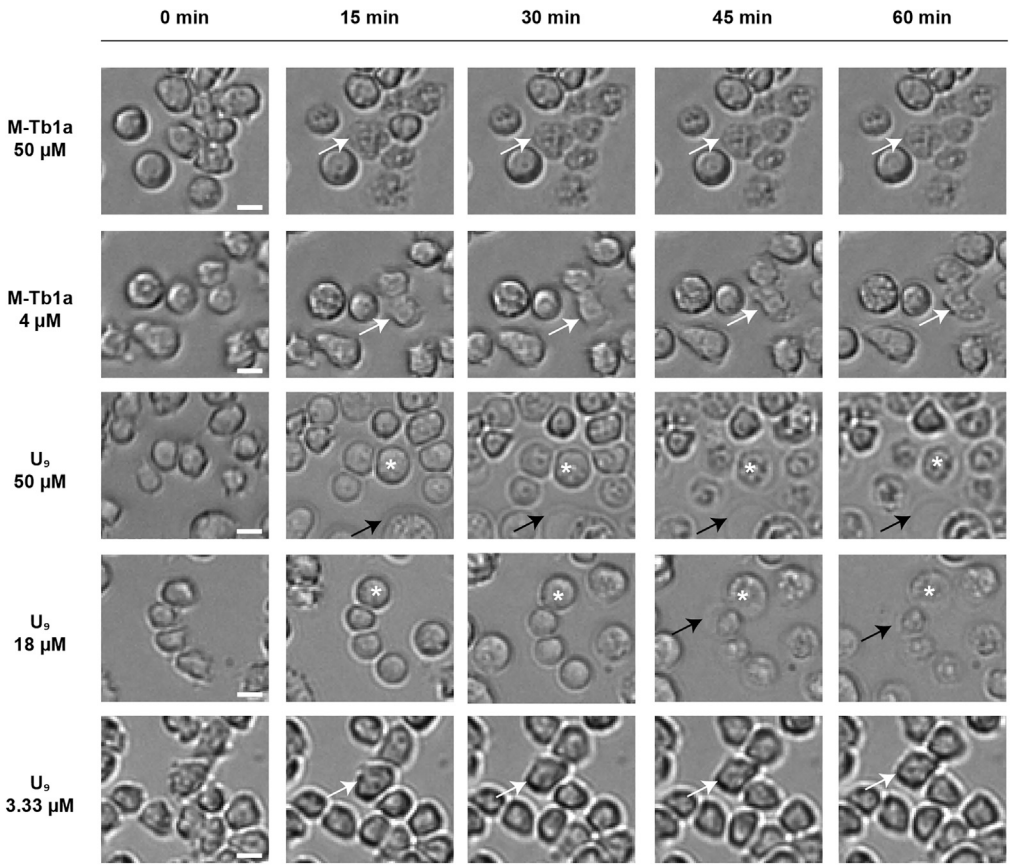

Figure 3. Evolution of morphotypes of S2 cells exposed to M-Tb1a or U_9 peptides

Evolution of treated S2 cells morphology for 1 h after exposure to graded concentrations of M-Tb1a and U_9 (white arrows indicate cells with morphological changes; black arrows show membrane blebs; asterisks indicate cell swelling). Scale bar: 10 µm. See also Video S1.

predominantly dense with a radius of approximately 300–500 nm (Figure 6). No visible effect on mitochondria was observed after exposure to M-Tb1a at 4 µM before 2 h, where a few cells exhibited a small decrease in mitochondria density (Figure 6). In contrast, at lytic and sublytic LC_{50}, after the same exposure time, U_9 induced swelling (radius of about 500–800 nm) and disorganization of mitochondria, including the disappearance of mitochondrial cristae (Figure 6). In addition, for a few cells, after exposure to U_9 at lytic and sublytic LC_{50}, we observed mitochondrial membrane rupture (Figure 6). Thus, U_9 induced greater mitochondrial damages than M-Tb1a.

Dcp-1/drICE caspase activation by U_9-MYRTX-Tb1a

As in mammals, *Drosophila* mitochondria are involved in the apoptosis pathway. Therefore, U_9 induced alterations in mitochondria led us to monitor the activation of *Drosophila* caspase-3 homologues (i.e., Death caspase-1 (Dcp-1) and Death related ICE-like caspase (Drice)). At 50 µM and lytic LC_{50}, U_9 induced a strong caspase activation similar to the cycloheximide (CHX) positive control (Figures 7A and 7B). Little to no caspase activation was observed at the sublytic LC_{50} and 1 µM, respectively (Figure 7B). These results showed a concentration-dependent effect of U_9 for Dcp-1/Drice caspase activation. For M-Tb1a, all concentrations induced weak caspase activation. (Figures 7A and 7B).

Cytotoxic activity of U_9 is caspase-independent

To determine the role of caspase Dcp-1/Drice in U_9 activity, its cytotoxic effect was evaluated in the presence of Z-VAD-FMK (zVAD), a non-specific caspase inhibitor. As expected, the cytotoxic effect of CHX was decreased in the presence of zVAD (Figure 7C). For both peptides, no additional effect on cytotoxicity was

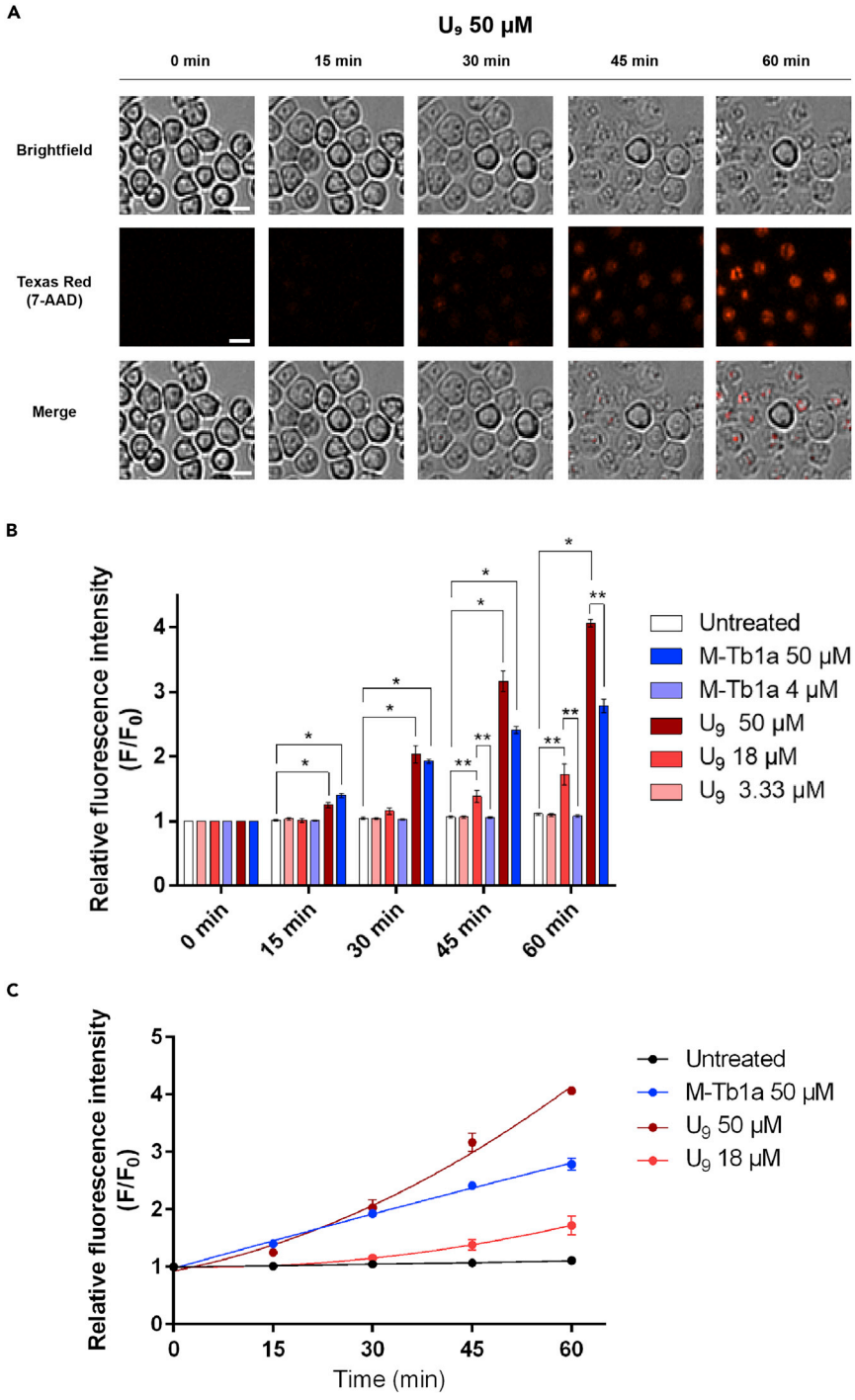

Figure 4. Permeabilization effects of M-Tb1a and U_9 peptides on S2 cells

Cell permeabilization was monitored by the entry of 7-AAD dye and binding to the nucleus.

(A) Cell morphotypes and 7-AAD uptake during exposure to U_9 at 50 µM for 1h.

(B and C) Relative fluorescence intensity during 1h exposure with either peptide at high concentration (50 µM), LC_{50} (4 or 18 µM), and sublytic concentration (3.33 µM). Values are represented with mean ± SEM Statistical analysis with Mann-Whitney (NS: $p > 0.05$, *: $p < 0.05$, **: $p < 0.01$) test (n = 3–5). Scale bar: 10 µm.

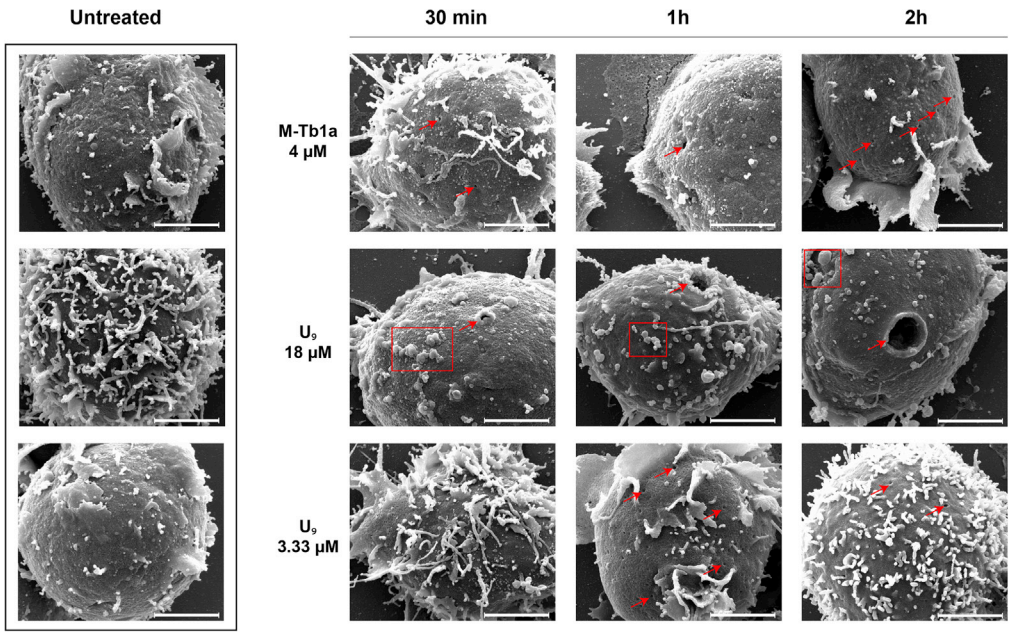

Figure 5. U_9 and M-Tb1a induced membrane pore formations

Pore formations observed by SEM after exposure to peptides during different exposure times: untreated; M-Tb1a at 4 µM; U_9 at 18 µM and 3.33 µM. Red arrows indicate pores. Red boxes indicate vesicle-like elements on the cell surface. Scale bar: 2 µm.

observed in the presence of zVAD, despite a slight of cell viability (U_9 at sublytic LC_{50} condition) or mortality (M-Tb1a at the lytic LC_{50} condition) (Figures 7C and 7D). These results demonstrated that the cytotoxic effect of U_9 is independent of caspases.

Localization of U9 peptide into S2 cells

The permeabilization of the cell membrane as well as the alteration of mitochondria suggests that U_9 could enter the exposed cells. We, therefore, examined the localization of U_9 after different incubation times with S2 cells. Immunolocalization of non-permeabilized S2 cells showed accumulation of U_9 at the membrane over a restricted area for all conditions (Figure 8). As expected, the accumulation area is larger at 18 µM than at 3.33 µM. Furthermore, at the lytic LC_{50}, peptide accumulation increases as a function of time. In parallel, immunostaining of permeabilized cells after exposure to 18 µM showed a higher intracellular fluorescence than untreated cells for all conditions (Figure 9) suggesting an entry of U_9 into the S2 cells. On the other hand, we did not detect the presence of U_9 in cells after exposure at the sublytic LC_{50} (data not shown). These results demonstrated that U_9 peptide at lytic LC_{50} accumulated at the membrane level but probably also into cells. Furthermore, exposure to U_9 at 18 µM induced a significant change in the organization of actin cytoskeleton for all exposure times in comparison with untreated cells (Figures 8 and 9). For several cells, actin vesicles-like were observed (Figures 8 and 9). At 3.33 µM, a slight decrease in phalloidin staining compared with control was observed for all exposure times, suggesting the onset of actin cytoskeleton disorganization (Figure 8).

NMR structure of U_9 peptide

To better understand the mode of action of U_9 at the molecular level, the 3D-structure of U9 was determined by nuclear magnetic resonance (NMR). A total of 346 nuclear overhauser effect (NOE)-derived distance restraints, 9 hydrogen bonds and 30 dihedral angles were considered (Table S1). The 15 lowest-energy structures exhibited similar backbone folding with a Root-Mean-Square Deviation (RMSD) of approximately 0.45 Å. The structure of U_9 is composed of two α-helices (α1: Ile2-Lys10 and α2: Val12-Ala17) connected by a flexible hinge around Lys10-Gly11-Val12 and forming an angle of - (97 $\pm$ 3)° (Figures 10 and S2). The side chains of the hydrophobic residues Ile2, Leu6, Leu13 and Met17 form a very stable hydrophobic core inside the concave face of the helix-turn-helix motif (HTH) (Figure S3A). U_9 adopts an

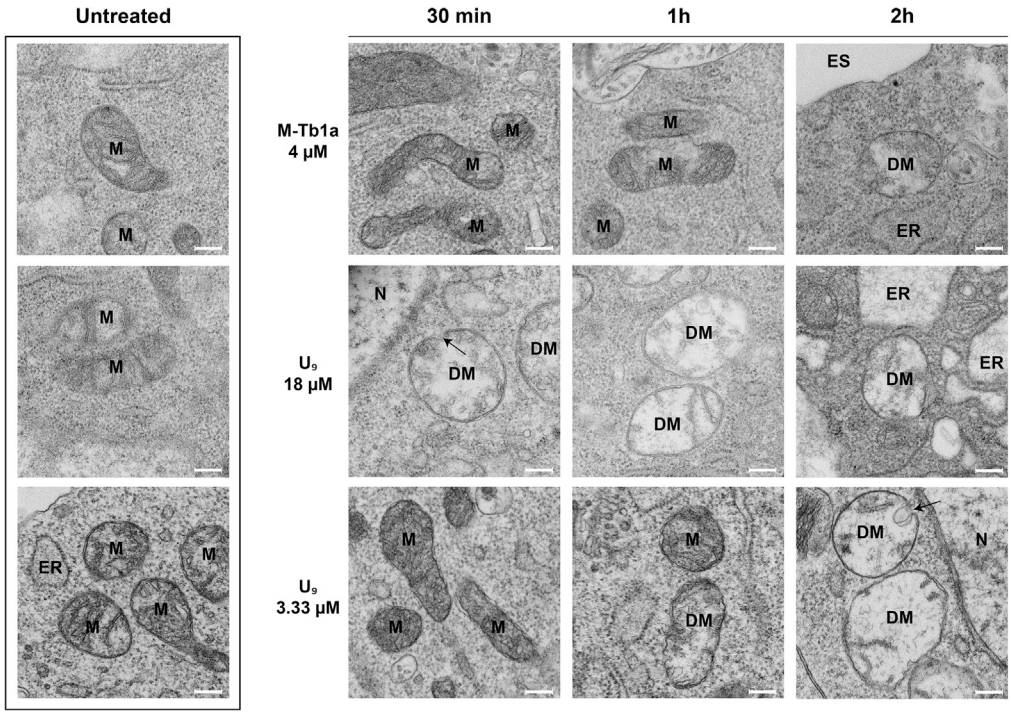

Figure 6. Mitochondrial damage induced by U_9

TEM analysis of mitochondrial morphotypes of untreated or treated S2 cells for different exposure times (30 min to 2h): M-Tb1a at 4 µM; U_9 at 18 µM or at 3.33 µM. M: Mitochondria; DM: damaged mitochondria; ES: extracellular space; N: nucleus; ER: ER Black arrows: membrane rupture. Scale bar: 200 nm.

amphipathic helical structure because its five lysine residues side chains are exposed to the solvent and spread on the same side of the molecular surface including the convex side of the hinge (Figure S3B). Hydrophobic amino acids are segregated on the opposite side of U_9 (Figure S3A). A similar fold of U_9 was obtained in sodium dodecyl sulfate (SDS) micelles (100 mM SDS-d25 at 318K) (data not shown).

Because the activity and pharmacology of U_9 are compared throughout the present study with those of M-Tb1a whose 3D structure was determined previously,[34] we have a refined 3D-structure of M-Tb1a. A total of 308 distance restraints instead of 156 were used for these calculations (Table S2). Overall, M-Tb1a forms a partially amphiphilic helix with a significant positive charge mainly in its N-terminal part and a narrow hydrophobic motif extended over $^1/_3$ of the peptide surface (Figure S4).

DISCUSSION

In this study, we demonstrated that both M-Tb1a and U_9 are cytotoxic to insect cells and that the cytotoxicity of U_9 involves interactions with the cell membrane and intracellular targets such as mitochondria. So far, only peptides from vertebrate (e.g., cardiotoxins) or invertebrate venoms such as aculeatoxins (e.g., melittin, mastoparan) have shown cytotoxic effects on mitochondria.[36] Our investigation is the first study described a mitochondrial damaging peptide isolated from ant venom.

Paralytic and cytotoxic activities of U_9 and M-Tb1a against insects

In addition to a paralyzing effect on blowflies, U_9 and M-Tb1a have been shown to have cytotoxic activity at 24 h on *Drosophila* S2 cells. As cytotoxic peptides, they participate in the offensive role of the venom by inducing paralysis of the prey insect, as has been reported for other membrane-active venom peptides.[26,27] So far, the effects of several peptides from various venoms (from Hymenoptera,[10,11,13–15,26,27,37–41] spiders,[42,43] scorpions[44] ...) have been evaluated on insects using *in vivo* assays. However, few studies have focused on insect cells[16,38,45–47] despite the relevance of this cellular model to elucidate the mode of action of cytotoxic peptides, to exploit the diversity of peptide libraries to discover new insecticides,

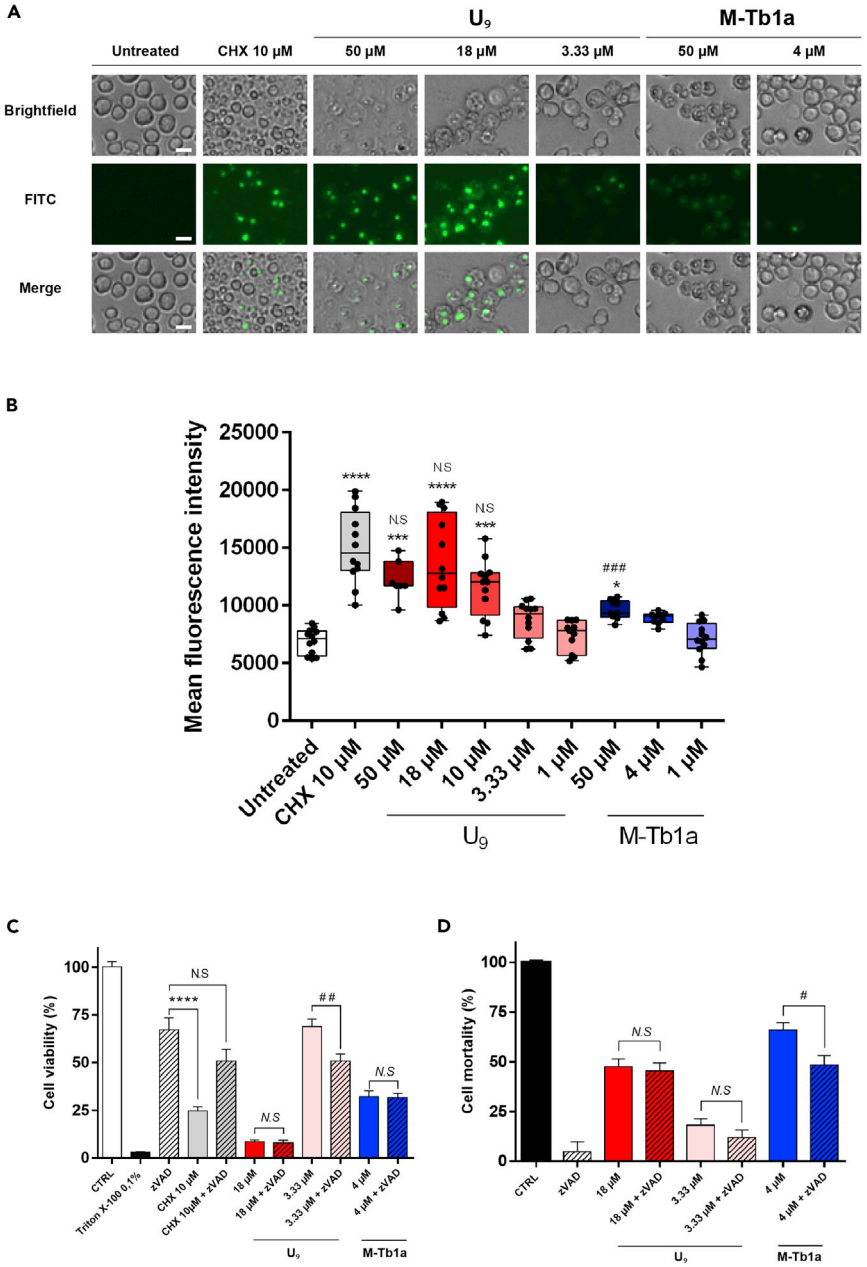

Figure 7. Dcp1/DrICE caspase activation and U_9-induced caspase-independent cytotoxic effect on S2 cells

(A) Fluorescence of S2 cells after caspase activation induced by 24h exposure to M-Tb1a or U_9 at high (50 µM), LC_{50} (4 or 18 µM) and sublytic (3.33 µM) concentration. Scale bar: 10 µm.

(B) Mean fluorescence intensity after exposure to peptide at different concentrations ranging from 50 µM to 1 µM, or CHX at 10 µM for 24h. Values are represented by a box and whiskers including replicates. Statistical analysis with Kruskal-Wallis test in comparison with Untreated (*: $p < 0.05$, ***: $p < 0.01$; ****: $p < 0.0001$) or CHX (N.S: $p > 0.05$, ###: $p < 0.001$) conditions (n = 7–12).

(C and D) Cytotoxic activity of U_9 and M-Tb1a peptides with or without the 100 µM caspase inhibitor zVAD measured by CCK-8 (C) and LDH (D) assays. Data were normalized to control according to the manufacturer's recommendations and represented as mean ± SEM Statistical analysis with Kruskal-Wallis (N.S: $p > 0.05$, ****: $p < 0.0001$) or t-student (*N.S*: $p > 0.05$, #: $p < 0.01$, ##: $p < 0.001$) tests (n = 9–12).

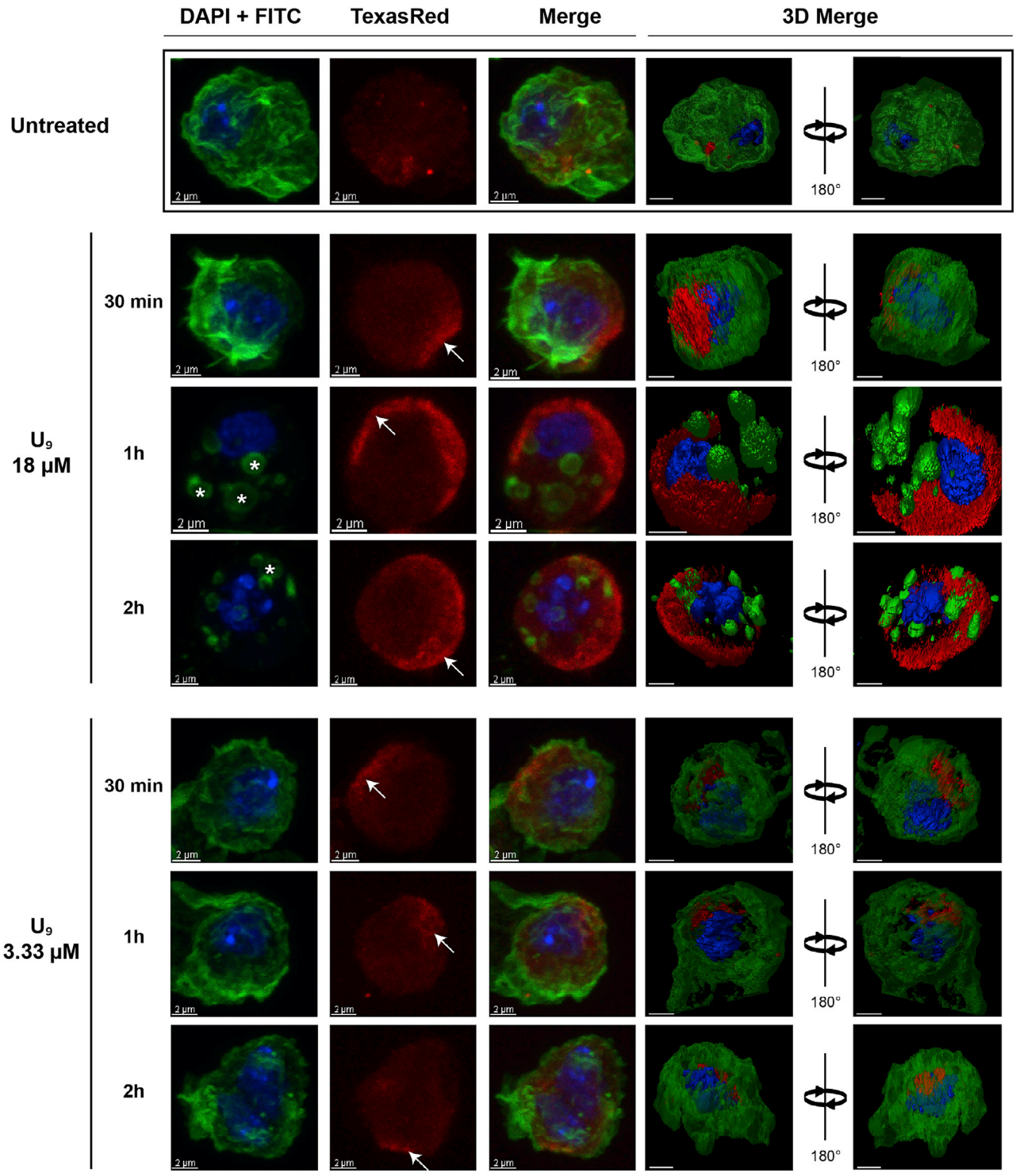

Figure 8. Localization of U_9 peptide at the membrane after exposure to non-permeabilized S2 cells

Indirect immunocytochemistry visualization by binding anti-U_9 antibody the membrane of non-permeabilized cells: DAPI and FITC show the nucleus and cytoskeleton of S2 cells, respectively. TexasRed shows the non-specific binding sites of the anti-U_9 primary antibody for untreated cells and the localization of U_9 for cells treated with the peptide at 18 µM and 3.33 µM for various exposure times (30 min to 2h). White arrows indicate U_9 peptide localization; asterisks indicate actin vesicles-like. Scale bar: 2 µm.

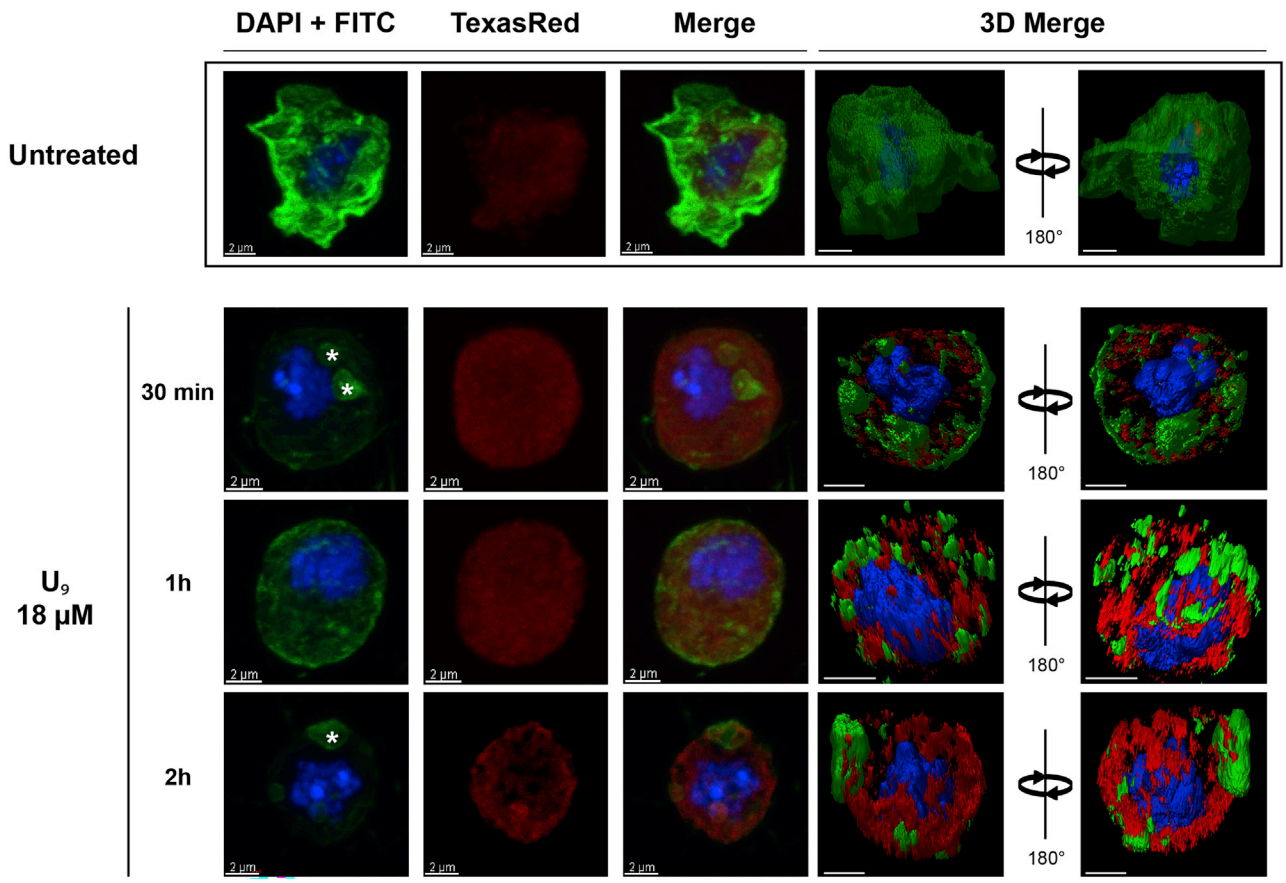

Figure 9. U_9 peptide entry into the permeabilized S2 cells

Indirect immunocytochemistry visualization by binding anti-U_9 antibody in permeabilized cells: DAPI and FITC show the nucleus and cytoskeleton of S2 cells, respectively. TexasRed shows the non-specific binding sites of anti-U_9 primary antibody for untreated cells and the localization of U_9 for cells treated with the 18 µM peptide for various exposure times (30 min to 2h). Asterisks show actin vesicles-like. Scale bar: 2 µm.

or to extend the knowledge of the functions of venom peptides. U_9 and M-Tb1a have a cytotoxic effect on S2 cells as potent as that of the previously studied ant venom cytotoxic peptides.[38,46]

Until now, cytotoxicity assays were mainly conducted using only one type of assay among cell lysis (LDH) and viability (MTT, XTT, CCK-8), an approach that does not allow the identification of cytotoxic peptides with novel mechanisms of action. In this study, we combined a viability assay (CCK-8) with a cell lysis assay (LDH) to investigate the effect of M-Tb1a and U_9 peptides on cell metabolism. This strategy proved to be relevant as it revealed different mechanisms of cell death. The cytotoxic mechanism of U_9 against S2 cells first impacts cell metabolism and then induces concentration-dependent cell lysis.

Cell membrane level: Permeabilization through pore-forming

SEM experiments allowed us to advance in the understanding of the cytotoxic mechanisms of U_9 because it induced two distinct membrane pore phenotypes depending on the concentration. M-Tb1a induced small pore formation at LC_{50} (4 µM) leading to cell lysis at 24 h.

Furthermore, for M-Tb1a at LC_{50} and U_9 at sublytic LC_{50}, no permeabilization to 7-AAD was observed, indicating that the small pores did not induce immediate cell permeabilization to 7-AAD molecules. A previous study demonstrated that M-Tb1a induced rapid permeabilization of the bacterial membrane to SYTOX green starting at approximately 1.4 µM for the most sensitive bacteria[34] (note that SYTOX green is a smaller compound than 7-AAD and therefore more likely to enter the cell). At the lytic LC_{50}, the large U_9-induced pores lead to rapid permeabilization to 7-AAD following an exponential kinetic profile that, to our knowledge, has not been described in the literature. The linear kinetic profile observed for M-Tb1a at 50 µM

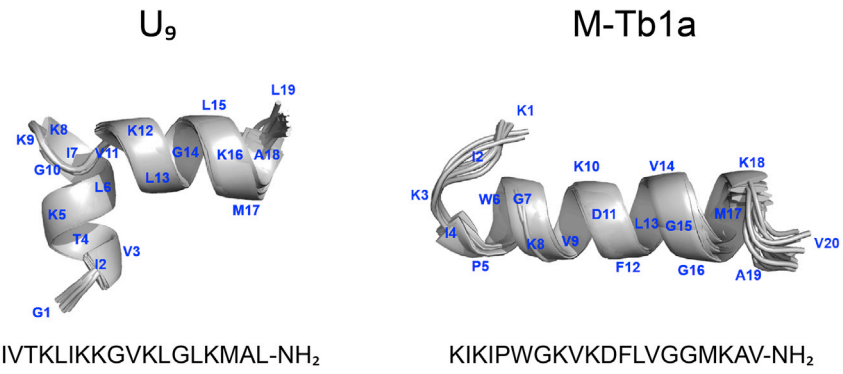

Figure 10. Solution structures of the U_9 and M-Tb1a peptides

For each peptide, the superimposed 15 lowest-energy structures are represented in cartoon. Amino acids are labeled in blue.

suggests another permeabilization mechanism. Indeed, depending on the peptides, kinetic profiles can be modified and associated with different permeabilization models.[48] However, further biophysical studies would be necessary to establish the precise permeabilization models of both peptides. Nevertheless, the above observations raise questions about the mechanisms for pore formation induced by U_9 and M-Tb1a at the concentrations tested.

Currently, 19 mechanisms promoting pore formations[49,50] have been proposed, the most documented being the toroidal model, the barrel-stave model, the carpet model and the detergent model.[49,51–58] Immunolocalization experiments showed that, both at lytic and sublytic LC_{50}, U_9 accumulates on the cell membrane surface. Taken together, our observations support a detergent-like model, which consists of a carpet-like coating of the cell membrane followed by micelle-forming disruption of the bilayer, resulting in the formation of pore-like structures.[49,50] Such micelles could be assimilated to the vesicle-like structures that we observed on the cell surface using SEM (Figure 5). Moreover, in the detergent-like model, low concentrations of the peptide can induce minor membrane changes, which are described as "small and transient apertures" without formation of micelles.[49,50] Such a mechanism would explain at the difference in U9-induced pores at different concentrations. The ability of the two peptides to form different pore types probably depends on their amino acid compositions and 3D structures. M-Tb1a and U_9 are linear amphiphilic peptides whose 3D structures are a straight α-helix and a helix-hinge-helix, respectively. Many antimicrobial peptides that disrupt bacterial membranes adopt an amphipathic helical structure at the membrane interface and, for some, a helix-hinge-helix conformation.[59] The presence of a flexible loop or hinge in the middle of a helical peptide is often associated with enhanced antibacterial activity, presumably by allowing either or both of the N- and C-terminal groups to bind to the membrane, thereby facilitating the process of peptide penetration into lipid bilayers.[60] However, M-Tb1a and U_9 differ in some of their physicochemical properties: hydrophobic face, hydrophobic moment, and polar angle (Table 1). These factors influence how the peptides interact with the membrane and consequently the mechanism of pore formation, especially in eukaryotic cells because of the zwitterionic membrane and hydrophobic environment.[50,61,62] Therefore, these variations likely explain the different pore phenotypes observed between U_9 and M-Tb1a at LC_{50}.

Intracellular level: Degradation of mitochondria and activation of caspase-3 homologs

Alteration of mitochondria (swelling, membrane disruption) after exposure to U_9 is suggestive of peptide internalization. However, these effects were also observed at the sublytic LC_{50}, for which U_9 was not detected inside the cells and for which the pores were relatively small. Therefore, the detection limits of immunostaining method can be questioned: 3.33 μM is maybe a too low concentration to lead to an intracellular signal by immunolocalization. Further investigations on localization of U_9 peptide by using methods with a better resolution can be considered such as mass spectrometer method.[63,64] The potential translocation of the peptide into cells is also consistent with the detergent-like model where peptide internalization is promoted by micellization.[53,55,58,65,66]

Although mitochondria have been extensively studied for their role in apoptosis, little is known about mitochondrial swelling.[67] Yet, changes in homeostasis and matrix volume appear to drive this dynamic. In

Table 1. Comparison of structural and physicochemical properties of M-Tb1a and U_9 with other cytotoxic peptides

	M-Tb1a	U_9	Lt2a	Dk5a
Sequences	KIKIPWGKVKDFL VGGMKAV	GIVTKLIKKGVK LGLKMAL	GLFGKLIKKFGRKAI SYAVKKARGKH	RFGGILKILKKVLPKAIK VAAEMAPPQNE[a]
Structures[b]		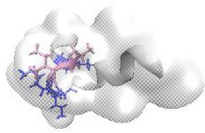	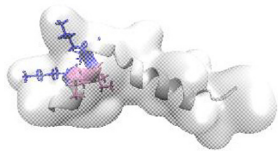	
Helical wheel[c]	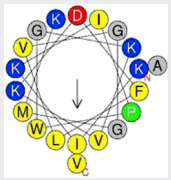	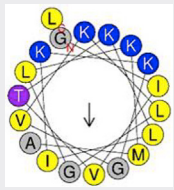	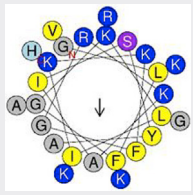	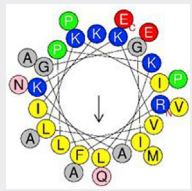
Hydrophobic Face[c]	FPGVIVLWM	ILLMGVGIAV	AGGAI	FALLAI
PTM	C-term amidation	C-term amidation		
Net charge[d]	5	6	9.1	4
pI[d]	11.28	14	11.73	10.83
H[c]	0.477	0.510	0.186	0.39
μ_H[c]	0.439	0.326	0.271	0.422

[a]Sequence according to Jensen et al..[25]

[b]Structures were determined by NMR (M-Tb1a and U_9 in this study, Lt2a from Dubovskii et al.[60]) except for Dk5a, which was achieved using PepFold3.5 (https://mobyle.rpbs.univ-paris-diderot.fr/cgi-bin/portal.py#forms::PEP-FOLD3).

[c]The helical wheel, hydrophobic face, hydrophobicity (H) and hydrophobic moment (μ_H) were predicted with Heliquest tool (https://heliquest.ipmc.cnrs.fr/); arrow indicates the hydrophobic face.

[d]The isoelectric point (pI) and net charge were calculated with PepCalc (https://pepcalc.com/).

mammals, swelling is related to the modulation of ion channels localized in the inner mitochondrial membrane (IMM) (especially for K^+, Ca^{2+} fluxes), to the "opening" of the permeability transition pore, to the decrease of mitochondrial potential, to the modulation of water flux by aquaporins in the IMM[67,68] or to the permeabilization of the outer mitochondrial membrane (OMM) by peptides.[36,69]

In *Drosophila*, mitochondrial permeabilization is the main cause of the swelling phenotype, which could be induced by pore formation in the OMM or by activation of pro-apoptotic proteins such as RHG (Rip, Hid, Grim).[70,71] The osmotic shock induced by U_9 at 18 μM (cell swelling) could induce an ionic imbalance between the cytoplasm and the mitochondrial matrix, which could also participate in mitochondrial permeabilization since we observed a significant activation of caspase-3 homologues (Drice and Dcp-1) at 18 μM (Figure 7). Several studies have shown a major involvement of RHG proteins in caspase activation of via the degradation of Death-associated inhibitor of apoptosis 1 (Diap1), an inhibitor of apoptosis.[70–72]

Mitochondrial permeabilization could also promote caspase activation through the release of pro-apoptotic proteins such as cytochrome *c* and the high temperature requirement protein A2 (dOmi/HtrA2). Even though their involvement in apoptosis is still unclear and controversial, these proteins play a minor role in the activation of Drice/Dcp-1 caspases.[71,73] However, we could demonstrate that inhibition of caspase activation had no effect on the cytotoxic activity of the U_9 peptide (Figure 7), showing that its impact on mitochondrial physiology is independent of apoptosis. A similar effect was also observed for the spider *Lachesana tarabaevi* venom peptide M-ZDTX-Lt2a (Lt2a) against human cells, which formed small pores, followed by a peptide accumulation into mitochondria triggering their inactivation and apoptosis-independent phosphatidylserine externalization.[74] U_9 and Lt2a share a similar 3D structure and the "KLIKK" motif (Table 1, Figures S5 and S6) that might be involved in their biological activity since its modification led to a significant decrease in the activity of Lt2a against some biological targets

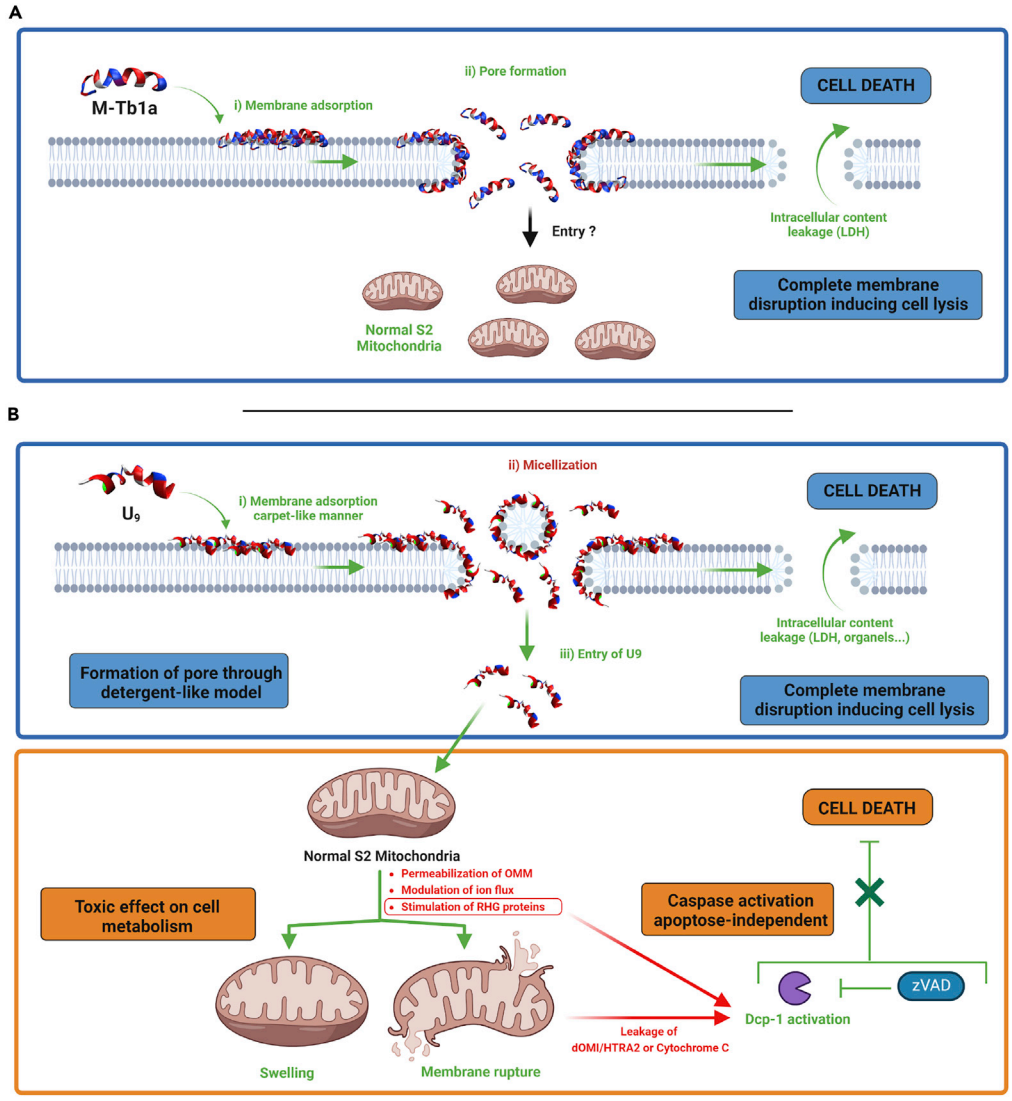

Figure 11. Presumable pathway of M-Tb1a and U9 cytotoxicity

(A) potential mechanism of M-Tb1a against S2 cells via pore formation leading to a complete membrane disruption. (B) potential mechanism of U9 against S2 cells including a necrosis part and an apoptosis-like part framed in blue and orange respectively. The green elements are based on experimental data from this study whereas the red elements are based on theoretical data from the literature. Created with BioRender.com.

(erythrocytes and leukocytes).[75] Dk5a, another pore-forming peptide characterized by the venom of the parasitoid velvet ant *Dasymutilla klugii* also shares these structural features[25] (Table 1).

Taken together, our results support a classical necrosis pathway for M-Tb1a peptide (Figure 11A) and a novel mechanism of action for U_9 (Figure 11B) leading to cell death. The peptide could aggregate in a carpet-like manner with its hydrophobic side on the S2 cell membrane. At sublytic LC_{50} (3.33 μM), the peptide induces transient apertures evidenced by the presence of small pores, whereas at lytic LC_{50} the distortion of the cell membrane promotes micellization, inducing the formation of large pores. Then, U_9 enters the cells, probably through the pores, leading to subsequent permeabilization of mitochondria by pore formation or stimulation of RHG proteins. In parallel, peptide accumulation and micellization of the S2 cell membrane eventually lead to its complete rupture and cell lysis. This proposed mechanism of action suggests that U_9 would follow a pathway between necrosis and apoptosis. It should be noted that such a mechanism involving membrane disruption followed by mitochondrial alteration had been previously described for

peptides from other venoms called mitochondriotoxins[36] but has not been reported for ant venom peptides. However, further studies on U_9 will be necessary to confirm the mechanism, especially on mitochondria.

Biological significances

We follow the standard nomenclature proposed for naming peptides from ant venoms.[9] Until now, no studies have been conducted on the biological activity of U_9, which explains the "U" prefix. In this study, we have clearly demonstrated that U_9 interacts with the cell membrane to induce cytotoxicity. Based on this study and current nomenclature, we propose to rename U_9 as M-MYRTX-Tb2a, where "M" stands for membrane perturbating. This compound is the second membrane-active peptide from *T. bicarinatum* venom. Its different mode of action from that of M-Tb1a highlights the functional and pharmacological diversification of aculeatoxin peptides to achieve lethal venom cocktails likely promoted by selective pressures. The distinctive mode of action of peptides with the same function is an evolutionary advantage that prevents prey resistance mechanisms. It would also be interesting to study the synergistic activity of these two peptides against prey. Besides, mitochondria are the main biological targets for various therapeutic applications. Although further studies will be necessary to specify the mechanism of M-MYRTX-Tb2a, one can wonder about the potential valorizations of this peptide targeting mitochondria. This investigation is consistent with previous studies pointing out that ants and all hymenopterans are experts at disrupting the cell membrane through a wide panel of venom peptides. Hymenopteran venoms thus provide a vast source of membrane-active molecules that warrant investigation for various applications.

Limitations of the study

This study demonstrated that U_9 peptide causes formation of pores at membrane level and could enter into S2 cells. Nevertheless, we could not relate the presence of membrane pores (SEM analysis) to permeabilization events at membrane level (no 7-AAD permeabilization and no osmotic change observable) at 3.33 μM. Further experiments with more sensitive methods (e.g., ion flux measurements) could provide additional data to answer this question. Regarding the localization of U_9 at 18 μM, further experiments will be required to clarify intracellular localization and potential accumulation in an intracellular organelle such as mitochondria. Finally, in this study U_9 and M-Tb1a mechanisms were compared whereas only U_9 localization was tested. However, M-Tb1a is also a pore-former peptide, so it would be interesting to study its localizations at both membrane and intracellular levels and compared them to U_9 peptide.

STAR★METHODS

Detailed methods are provided in the online version of this paper and include the following:

- KEY RESOURCES TABLE
- RESOURCE AVAILABILITY
  - Lead contact
  - Materials availability
  - Data and code availability
- EXPERIMENTAL MODEL AND SUBJECT DETAILS
  - Insect
  - Insect cell line
- METHOD DETAILS
  - Peptides
  - *In vivo* insecticidal assays
  - Cytotoxicity assays
  - Membrane permeabilization assay
  - Preparation of cell samples for SEM and TEM observations
  - Monitoring of Caspase-3 homolog (Drice/Dcp-1)
  - Immunocytochemistry
  - NMR experiments
  - Structure calculations
- QUANTIFICATION AND STATISTICAL ANALYSIS
  - Data and statistical analysis

SUPPLEMENTAL INFORMATION

Supplemental information can be found online at https://doi.org/10.1016/j.isci.2023.106157.

ACKNOWLEDGMENTS

S.A. was the recipient of a PhD fellowship from the Région Occitanie (France) and the University Champollion. Thanks to the Drosophila Genomics Resource Center, supported by NIH grant 2P40OD010949, and in particular, Dr. Arthur Luhur for his helpful advice on maintaining S2 cells. Thanks to CMEAB (Faculté de Médecine Rangueil, Toulouse, France), in particular Isabelle Fourquaux and FRAIB-TRIImaging Plat-form Facilities (FR AIB, Université deToulouse, CNRS, 31320 Castanet-Tolosan, France) for their assistance in capture of electron microscope and confocal images respectively. Thanks to the NMR division of the MO2VING facility (Orléans, France). Finally, we would like to thank Gladys Donald (Cambridge Proofreading) for polishing the English.

AUTHOR CONTRIBUTIONS

Conceptualization: S.A., A.T., N.T., F.P., M.T., A.B., and E.B.; Methodology: S.A., A.T., F.P., M.T., A.B., and E.B.; Validation: S.A., M.T., A.B., and E.B.; Formal Analysis: S.A., A.T., and F.P; Investigation: S.A., A.T., and F.P.; Resources: J.L. and B.L.; Writing – Original Draft: S.A., A.T., F.P., M.T., A.B., and E.B.; Writing – Review and Editing: S.A., N.T., A.T., J.L., F.P., L.J., V.B., M.T., A.B., and E.B.; Visualization: S.A., A.T., F.P.,M.T., A.B., and E.B.; Supervision: M.T., A.B., and E.B.; Funding Acquisition, M.T. and E.B.

DECLARATION OF INTERESTS

The authors declare no competing interests.

Received: November 22, 2022
Revised: January 17, 2023
Accepted: February 2, 2023
Published: February 8, 2023

REFERENCES

1. Bordon, K.d.C.F., Cologna, C.T., Fornari-Baldo, E.C., Pinheiro-Júnior, E.L., Cerni, F.A., Amorim, F.G., Anjolette, F.A.P., Cordeiro, F.A., Wiezel, G.A., Cardoso, I.A., et al. (2020). From animal poisons and venoms to medicines: achievements, challenges and perspectives in drug discovery. Front. Pharmacol. *11*, 1132. https://doi.org/10.3389/fphar.2020.01132.

2. Herzig, V., Cristofori-Armstrong, B., Israel, M.R., Nixon, S.A., Vetter, I., and King, G.F. (2020). Animal toxins — nature's evolutionary-refined toolkit for basic research and drug discovery. Biochem. Pharmacol. *181*, 114096. https://doi.org/10.1016/j.bcp.2020.114096.

3. Pennington, M.W., Czerwinski, A., and Norton, R.S. (2018). Peptide therapeutics from venom: current status and potential. Bioorg. Med. Chem. *26*, 2738–2758. https://doi.org/10.1016/j.bmc.2017.09.029.

4. Smallwood, T.B., and Clark, R.J. (2021). Advances in venom peptide drug discovery: where are we at and where are we heading? Expet Opin. Drug Discov. *16*, 1163–1173. https://doi.org/10.1080/17460441.2021.1922386.

5. Yacoub, T., Rima, M., Karam, M., Sabatier, J.M., and Fajloun, Z. (2020). Antimicrobials from venomous animals: an overview. Molecules *25*, 2402. https://doi.org/10.3390/molecules25102402.

6. Aili, S.R., Touchard, A., Escoubas, P., Padula, M.P., Orivel, J., Dejean, A., and Nicholson, G.M. (2014). Diversity of peptide toxins from stinging ant venoms. Toxicon *92*, 166–178. https://doi.org/10.1016/j.toxicon.2014.10.021.

7. Touchard, A., Koh, J.M.S., Aili, S.R., Dejean, A., Nicholson, G.M., Orivel, J., and Escoubas, P. (2015). The complexity and structural diversity of ant venom peptidomes is revealed by mass spectrometry profiling. Rapid Commun. Mass Spectrom. *29*, 385–396. https://doi.org/10.1002/rcm.7116.

8. Walker, A.A., Robinson, S.D., Yeates, D.K., Jin, J., Baumann, K., Dobson, J., Fry, B.G., and King, G.F. (2018). Entomo-venomics: the evolution, biology and biochemistry of insect venoms. Toxicon *154*, 15–27. https://doi.org/10.1016/j.toxicon.2018.09.004.

9. Touchard, A., Aili, S.R., Fox, E.G.P., Escoubas, P., Orivel, J., Nicholson, G.M., and Dejean, A. (2016). The biochemical toxin arsenal from ant venoms. Toxins *8*, 30. https://doi.org/10.3390/toxins8010030.

10. Guido-Patiño, J.C., and Plisson, F. (2022). Profiling hymenopteran venom toxins: protein families, structural landscape, biological activities, and pharmacological benefits. Toxicon X *14*, 100119. https://doi.org/10.1016/j.toxcx.2022.100119.

11. Orivel, J., Redeker, V., Le Caer, J.P., Krier, F., Revol-Junelles, A.M., Longeon, A., Chaffotte, A., Dejean, A., and Rossier, J. (2001). Ponericins, new antibacterial and insecticidal peptides from the venom of the ant pachycondyla goeldii. J. Biol. Chem. *276*, 17823–17829. https://doi.org/10.1074/jbc.M100216200.

12. Senetra, A.S., Necelis, M.R., and Caputo, G.A. (2020). Investigation of the structure-activity relationship in ponericin L1 from Neoponera goeldii. Pept. Sci. *112*, e24162. https://doi.org/10.1002/pep2.24162.

13. Heep, J., Skaljac, M., Grotmann, J., Kessel, T., Seip, M., Schmidtberg, H., and Vilcinskas, A. (2019). Identification and functional characterization of a novel insecticidal decapeptide from the myrmicine ant manica rubida. Toxins *11*, 562. https://doi.org/10.3390/toxins11100562.

14. Touchard, A., Aili, S.R., Téné, N., Barassé, V., Klopp, C., Dejean, A., Kini, R.M., Mrinalini, C.L., Coquet, L., Jouenne, T., et al. (2020). Venom peptide repertoire of the European myrmicine ant manica rubida : identification of insecticidal toxins. J. Proteome Res. *19*, 1800–1811. https://doi.org/10.1021/acs.jproteome.0c00048.

15. Nixon, S.A., Robinson, S.D., Agwa, A.J., Walker, A.A., Choudhary, S., Touchard, A., Undheim, E.A.B., Robertson, A., Vetter, I., Schroeder, C.I., et al. (2021). Multipurpose

peptides: the venoms of Amazonian stinging ants contain anthelmintic ponericins with diverse predatory and defensive activities. Biochem. Pharmacol. *192*, 114693. https://doi.org/10.1016/j.bcp.2021.114693.

16. Piek, T., Duval, A., Hue, B., Karst, H., Lapied, B., Mantel, P., Nakajima, T., Pelhate, M., and Schmidt, J.O. (1991). Poneratoxin, a novel peptide neurotoxin from the venom of the ant, paraponera clavata. Comp. Biochem. Physiol. C Comp. Pharmacol. Toxicol. *99*, 487–495. https://doi.org/10.1016/0742-8413(91)90276-Y.

17. Szolajska, E., Poznanski, J., Ferber, M.L., Michalik, J., Gout, E., Fender, P., Bailly, I., Dublet, B., and Chroboczek, J. (2004). Poneratoxin, a neurotoxin from ant venom: structure and expression in insect cells and construction of a bio-insecticide. Eur. J. Biochem. *271*, 2127–2136. https://doi.org/10.1111/j.1432-1033.2004.04128.x.

18. Johnson, S.R., Copello, J.A., Evans, M.S., and Suarez, A.V. (2010). A biochemical characterization of the major peptides from the Venom of the giant Neotropical hunting ant Dinoponera australis. Toxicon *55*, 702–710. https://doi.org/10.1016/j.toxicon.2009.10.021.

19. Cologna, C.T., Cardoso, J.d.S., Jourdan, E., Degueldre, M., Upert, G., Gilles, N., Uetanabaro, A.P.T., Costa Neto, E.M., Thonart, P., de Pauw, E., et al. (2013). Peptidomic comparison and characterization of the major components of the venom of the giant ant Dinoponera quadriceps collected in four different areas of Brazil. J. Proteonomics *94*, 413–422. https://doi.org/10.1016/j.jprot.2013.10.017.

20. Dodou Lima, H.V., de Paula Cavalcante, C.S., and Rádis-Baptista, G. (2020). Antifungal in vitro activity of pilosulin- and ponericin-like peptides from the giant ant dinoponera quadriceps and synergistic effects with antimycotic drugs. Antibiotics *9*, 354. https://doi.org/10.3390/antibiotics9060354.

21. Ràdis-Baptista, G., Dodou, H.V., Prieto-Da-Silva, Á.R.B., Zaharenko, A.J., Kazuma, K., Nihei, K.I., Inagaki, H., Mori-Yasumoto, K., and Konno, K. (2020). Comprehensive analysis of peptides and low molecular weight components of the giant ant Dinoponera quadriceps venom. Preprint at Biol. Chem. https://doi.org/10.1515/hsz-2019-397ja-01.

22. Lima, D.B., Torres, A.F.C., Mello, C.P., de Menezes, R.R., Sampaio, T.L., Canuto, J.A., da Silva, J.J.A., Freire, V.N., Quinet, Y.P., Havt, A., et al. (2014). Antimicrobial effect of Dinoponera quadriceps (Hymenoptera: formicidae) venom against Staphylococcus aureus strains. J. Appl. Microbiol. *117*, 390–396. https://doi.org/10.1111/jam.12548.

23. Monteiro, M.L., Lima, D.B., Freire, K.A., Nicolaski Pedron, C., Magalhães, E.P., Silva, B.P., García-Jareño, A.B., De Oliveira, C.S., Nunes, J.V.S., Marinho, M.M., et al. (2022). Rational design of a trypanocidal peptide derived from Dinoponera quadriceps venom. Eur. J. Med. Chem. *241*, 114624. https://doi.org/10.1016/j.ejmech.2022.114624.

24. Lima, D.B., Mello, C.P., Bandeira, I.C.J., Pessoa Bezerra de Menezes, R.R.P., Sampaio, T.L., Falcão, C.B., Morlighem, J.É.R.L., Rádis-Baptista, G., and Martins, A.M.C. (2018). The dinoponeratoxin peptides from the giant ant Dinoponera quadriceps display in vitro antitrypanosomal activity. Biol. Chem. *399*, 187–196. https://doi.org/10.1515/hsz-2017-0198.

25. Jensen, T., Walker, A.A., Nguyen, S.H., Jin, A.H., Deuis, J.R., Vetter, I., King, G.F., Schmidt, J.O., and Robinson, S.D. (2021). Venom chemistry underlying the painful stings of velvet ants (Hymenoptera: mutillidae). Cell. Mol. Life Sci. *78*, 5163–5177. https://doi.org/10.1007/s00018-021-03847-1.

26. Robinson, S.D., Kambanis, L., Clayton, D., Hinneburg, H., Corcilius, L., Mueller, A., Walker, A.A., Keramidas, A., Kulkarni, S.S., Jones, A., et al. (2021). A pain-causing and paralytic ant venom glycopeptide. iScience *24*, 103175. https://doi.org/10.1016/j.isci.2021.103175.

27. Robinson, S.D., Mueller, A., Clayton, D., Starobova, H., Hamilton, B.R., Payne, R.J., Vetter, I., King, G.F., and Undheim, E.A.B. (2018). A comprehensive portrait of the venom of the giant red bull ant, Myrmecia gulosa, reveals a hyperdiverse hymenopteran toxin gene family. Sci. Adv. *4*, eaau4640. https://doi.org/10.1126/sciadv.aau4640.

28. Duraisamy, K., Singh, K., Kumar, M., Lefranc, B., Bonnafé, E., Treilhou, M., Leprince, J., and Chow, B.K.C. (2022). P17 induces chemotaxis and differentiation of monocytes via MRGPRX2-mediated mast cell–line activation. J. Allergy Clin. Immunol. *149*, 275–291. https://doi.org/10.1016/j.jaci.2021.04.040.

29. Touchard, A., Téné, N., Song, P.C.T., Lefranc, B., Leprince, J., Treilhou, M., and Bonnafé, E. (2018). Deciphering the molecular diversity of an ant venom peptidome through a venomics approach. J. Proteome Res. *17*, 3503–3516. https://doi.org/10.1021/acs.jproteome.8b00452.

30. Benmoussa, K., Authier, H., Prat, M., AlaEddine, M., Lefèvre, L., Rahabi, M.C., Bernad, J., Aubouy, A., Bonnafé, E., Leprince, J., et al. (2017). P17, an original host defense peptide from ant venom, promotes antifungal activities of macrophages through the induction of C-type lectin receptors dependent on LTB4-Mediated PPARγ activation. Front. Immunol. *8*, 1650. https://doi.org/10.3389/fimmu.2017.01650.

31. Eales, M.G., Ferrari, E., Goddard, A.D., Lancaster, L., Sanderson, P., and Miller, C. (2018). Mechanistic and phenotypic studies of bicarinalin, BP100 and colistin action on Acinetobacter baumannii. Res. Microbiol. *169*, 296–302. https://doi.org/10.1016/j.resmic.2018.04.005.

32. Guzman, J., Téné, N., Touchard, A., Castillo, D., Belkhelfa, H., Haddioui-Hbabi, L., Treilhou, M., and Sauvain, M. (2017). Anti-helicobacter pylori properties of the ant-venom peptide bicarinalin. Toxins *10*, 21. https://doi.org/10.3390/toxins10010021.

33. Rifflet, A., Gavalda, S., Téné, N., Orivel, J., Leprince, J., Guilhaudis, L., Génin, E., Vétillard, A., and Treilhou, M. (2012). Identification and characterization of a novel antimicrobial peptide from the venom of the ant Tetramorium bicarinatum. Peptides *38*, 363–370. https://doi.org/10.1016/j.peptides.2012.08.018.

34. Téné, N., Bonnafé, E., Berger, F., Rifflet, A., Guilhaudis, L., Ségalas-Milazzo, I., Pipy, B., Coste, A., Leprince, J., and Treilhou, M. (2016). Biochemical and biophysical combined study of bicarinalin, an ant venom antimicrobial peptide. Peptides *79*, 103–113. https://doi.org/10.1016/j.peptides.2016.04.001.

35. Téné, N., Roche-Chatain, V., Rifflet, A., Bonnafé, E., Lefranc, B., Leprince, J., and Treilhou, M. (2014). Potent bactericidal effects of bicarinalin against strains of the Enterobacter and Cronobacter genera. Food Control *42*, 202–206. https://doi.org/10.1016/j.foodcont.2014.02.026.

36. Colella, F., Scillitani, G., and Pierri, C.L. (2021). Sweet as honey, bitter as bile: mitochondriotoxic peptides and other therapeutic proteins isolated from animal tissues, for dealing with mitochondrial apoptosis. Toxicology *447*, 152612. https://doi.org/10.1016/j.tox.2020.152612.

37. Pluzhnikov, K.A., Nol'de, D.E., Tertyshnikova, S.M., Sukhanov, S.V., Sobol', A.G., Torgov, M.I., Filippov, A.K., Arsen'ev, A.S., and Grishin, E.V. (1994). Strukturno-funktsional'noe issledovanie osnovnogo toksicheskogo komponenta iada murav'ia Estatomma tuberculatum. Bioorg. Khim. *20*, 857–871.

38. Touchard, A., Mendel, H.C., Boulogne, I., Herzig, V., Braga Emidio, N., King, G.F., Triquigneaux, M., Jaquillard, L., Beroud, R., De Waard, M., et al. (2020). Heterodimeric insecticidal peptide provides new insights into the molecular and functional diversity of ant venoms. ACS Pharmacol. Transl. Sci. *3*, 1211–1224. https://doi.org/10.1021/acsptsci.0c00119.

39. Arseniev, A.S., Pluzhnikov, K.A., Nolde, D.E., Sobol, A.G., Torgov, M.Y., Sukhanov, S.V., and Grishin, E.V. (1994). Toxic principle of selva ant venom is a pore-forming protein transformer. FEBS Lett. *347*, 112–116. https://doi.org/10.1016/0014-5793(94)00518-4.

40. Nixon, S.A., Dekan, Z., Robinson, S.D., Guo, S., Vetter, I., Kotze, A.C., Alewood, P.F., King, G.F., and Herzig, V. (2020). It takes two: dimerization is essential for the broad-spectrum predatory and defensive activities of the venom peptide Mp1a from the jack jumper ant Myrmecia pilosula. Biomedicines *8*, 185. https://doi.org/10.3390/BIOMEDICINES8070185.

41. Pluzhnikov, K.A., Kozlov, S.A., Vassilevski, A.A., Vorontsova, O.V., Feofanov, A.V., and Grishin, E.V. (2014). Linear antimicrobial peptides from Ectatomma quadridens ant venom. Biochimie *107*, 211–215. https://doi.org/10.1016/j.biochi.2014.09.012.

42. Alvarado, D., Cardoso-Arenas, S., Corrales-García, L.L., Clement, H., Arenas, I., Montero-

Dominguez, P.A., Olamendi-Portugal, T., Zamudio, F., Csoti, A., Borrego, J., et al. (2020). A novel insecticidal spider peptide that affects the mammalian voltage-gated ion channel hKv1.5. Front. Pharmacol. *11*, 563858. https://doi.org/10.3389/fphar.2020.563858.

43. Nakasu, E.Y.T., Williamson, S.M., Edwards, M.G., Fitches, E.C., Gatehouse, J.A., Wright, G.A., and Gatehouse, A.M.R. (2014). Novel biopesticide based on a spider venom peptide shows no adverse effects on honeybees. Proc. Biol. Sci. *281*, 20140619. https://doi.org/10.1098/rspb.2014.0619.

44. Krämer, J., Lüddecke, T., Marner, M., Maiworm, E., Eichberg, J., Hardes, K., Schäberle, T.F., Vilcinskas, A., and Predel, R. (2022). Antimicrobial, insecticidal and cytotoxic activity of linear venom peptides from the pseudoscorpion chelifer cancroides. Toxins *14*, 58. https://doi.org/10.3390/toxins14010058.

45. Ji, S.J., Liu, F., Li, E.Q., and Zhu, Y.X. (2002). Recombinant scorpion insectotoxin AaIT kills specifically insect cells but not human cells. Cell Res. *12*, 143–150. https://doi.org/10.1038/sj.cr.7290120.

46. Pluzhnikov, K., Nosyreva, E., Shevchenko, L., Kokoz, Y., Schmalz, D., Hucho, F., and Grishin, E. (1999). Analysis of ectatomin action on cell membranes. Eur. J. Biochem. *262*, 501–506. https://doi.org/10.1046/j.1432-1327.1999.00426.x.

47. Murugan, D., and Saini, G.K. (2019). Cytotoxic and lethal effects of recombinant β-BUTX-Lqq1a peptide against Lepidopteran insects and cell lines. Toxicol. Vitro *60*, 44–50. https://doi.org/10.1016/j.tiv.2019.05.005.

48. Wimley, W.C., and Hristova, K. (2019). The mechanism of membrane permeabilization by peptides: still an enigma. Aust. J. Chem. *73*, 96–103. https://doi.org/10.1071/CH19449.

49. Bertrand, B., Garduño-Juárez, R., and Munoz-Garay, C. (2021). Estimation of pore dimensions in lipid membranes induced by peptides and other biomolecules: a review. Biochim. Biophys. Acta Biomembr. *1863*, 183551. https://doi.org/10.1016/j.bbamem.2021.183551.

50. Lee, T.-H., Hall, K.N., and Aguilar, M.-I. (2016). Antimicrobial peptide structure and mechanism of action: a focus on the role of membrane structure. Curr. Top. Med. Chem. *16*, 25–39. https://doi.org/10.2174/1568026615666150703121700.

51. Alghalayini, A., Garcia, A., Berry, T., and Cranfield, C.G. (2019). The use of tethered bilayer lipid membranes to identify the mechanisms of antimicrobial peptide interactions with lipid bilayers. Antibiotics *8*, 12. https://doi.org/10.3390/antibiotics8010012.

52. Erdem Büyükkiraz, M., and Kesmen, Z. (2022). Antimicrobial peptides (AMPs): a promising class of antimicrobial compounds. J. Appl. Microbiol. *132*, 1573–1596. https://doi.org/10.1111/jam.15314.

53. Hale, J.D.F., and Hancock, R.E.W. (2007). Alternative mechanisms of action of cationic antimicrobial peptides on bacteria. Expert Rev. Anti Infect. Ther. *5*, 951–959. https://doi.org/10.1586/14787210.5.6.951.

54. Li, J., Koh, J.J., Liu, S., Lakshminarayanan, R., Verma, C.S., and Beuerman, R.W. (2017). Membrane active antimicrobial peptides: translating mechanistic insights to design. Front. Neurosci. *11*, 73. https://doi.org/10.3389/fnins.2017.00073.

55. Snyder, A.B., and Worobo, R.W. (2014). Chemical and genetic characterization of bacteriocins: antimicrobial peptides for food safety. J. Sci. Food Agric. *94*, 28–44. https://doi.org/10.1002/jsfa.6293.

56. Wimley, W.C. (2010). Describing the mechanism of antimicrobial peptide action with the interfacial activity model. ACS Chem. Biol. *5*, 905–917. https://doi.org/10.1021/cb1001558.

57. Wimley, W.C., and Hristova, K. (2011). Antimicrobial peptides: successes, challenges and unanswered questions. J. Membr. Biol. *239*, 27–34. https://doi.org/10.1007/s00232-011-9343-0.

58. Zhang, Q.Y., Yan, Z.B., Meng, Y.M., Hong, X.Y., Shao, G., Ma, J.J., Cheng, X.R., Liu, J., Kang, J., and Fu, C.Y. (2021). Antimicrobial peptides: mechanism of action, activity and clinical potential. Mil. Med. Res. *8*, 1–25. https://doi.org/10.1186/S40779-021-00343-2.

59. Joodaki, F., Martin, L.M., and Greenfield, M.L. (2021). Computational study of helical and helix-hinge-helix conformations of an antimicrobial peptide in solution by molecular dynamics and vibrational analysis. J. Phys. Chem. B *125*, 703–721. https://doi.org/10.1021/acs.jpcb.0c07988.

60. Dubovskii, P.V., Volynsky, P.E., Polyansky, A.A., Chupin, V.V., Efremov, R.G., and Arseniev, A.S. (2006). Spatial structure and activity mechanism of a novel spider antimicrobial peptide. Biochemistry *45*, 10759–10767. https://doi.org/10.1021/bi060635w.

61. Chakraborty, S., Chatterjee, R., and Chakravortty, D. (2022). Evolving and assembling to pierce through: evolutionary and structural aspects of antimicrobial peptides. Comput. Struct. Biotechnol. J. *20*, 2247–2258. https://doi.org/10.1016/j.csbj.2022.05.002.

62. Chen, Y., Guarnieri, M.T., Vasil, A.I., Vasil, M.L., Mant, C.T., and Hodges, R.S. (2007). Role of peptide hydrophobicity in the mechanism of action of α-helical antimicrobial peptides. Antimicrob. Agents Chemother. *51*, 1398–1406. https://doi.org/10.1128/AAC.00925-06.

63. Marinova, Z., Vukojević, V., Surcheva, S., Yakovleva, T., Cebers, G., Pasikova, N., Usynin, I., Hugonin, L., Fang, W., Hallberg, M., et al. (2005). Translocation of dynorphin neuropeptides across the plasma membrane: a putative mechanism of signal transmission. J. Biol. Chem. *280*, 26360–26370. https://doi.org/10.1074/jbc.M412494200.

64. Møller, L.H., Gabel-Jensen, C., Franzyk, H., Bahnsen, J.S., Stürup, S., and Gammelgaard, B. (2014). Quantification of pharmaceutical peptides using selenium as an elemental detection label. Metallomics *6*, 1639–1647. https://doi.org/10.1039/c4mt00085d.

65. Hancock, R.E.W., and Patrzykat, A. (2002). Clinical development of cationic antimicrobial peptides: from natural to novel antibiotics. Curr. Drug Targets: Infect. Disord. *2*, 79–83. https://doi.org/10.2174/1568005024605855.

66. Ruseska, I., and Zimmer, A. (2020). Internalization mechanisms of cell-penetrating peptides. Beilstein J. Nanotechnol. *11*, 101–123. https://doi.org/10.3762/bjnano.11.10.

67. Javadov, S., Chapa-Dubocq, X., and Makarov, V. (2018). Different approaches to modeling analysis of mitochondrial swelling. Mitochondrion *38*, 58–70. https://doi.org/10.1016/j.mito.2017.08.004.

68. Kaasik, A., Safiulina, D., Zharkovsky, A., and Veksler, V. (2007). Regulation of mitochondrial matrix volume. Am. J. Physiol. Cell Physiol. *292*, 157–163. https://doi.org/10.1152/ajpcell.00272.2006.

69. Von Stockum, S., Basso, E., Petronilli, V., Sabatelli, P., Forte, M.A., and Bernardi, P. (2011). Properties of Ca 2+ transport in mitochondria of Drosophila melanogaster. J. Biol. Chem. *286*, 41163–41170. https://doi.org/10.1074/jbc.M111.268375.

70. Abdelwahid, E., Yokokura, T., Krieser, R.J., Balasundaram, S., Fowle, W.H., and White, K. (2007). Mitochondrial disruption in Drosophila apoptosis. Dev. Cell *12*, 793–806. https://doi.org/10.1016/j.devcel.2007.04.004.

71. Clavier, A., Rincheval-Arnold, A., Colin, J., Mignotte, B., and Guénal, I. (2016). Apoptosis in Drosophila: which role for mitochondria? Apoptosis *21*, 239–251. https://doi.org/10.1007/s10495-015-1209-y.

72. Xu, D., Wang, Y., Willecke, R., Chen, Z., Ding, T., and Bergmann, A. (2006). The effector caspases drICE and dcp-1 have partially overlapping functions in the apoptotic pathway in Drosophila. Cell Death Differ. *13*, 1697–1706. https://doi.org/10.1038/sj.cdd.4401920.

73. Challa, M., Malladi, S., Pellock, B.J., Dresnek, D., Varadarajan, S., Yin, Y.W., White, K., and Bratton, S.B. (2007). Drosophila Omi, a mitochondrial-localized IAP antagonist and proapoptotic serine protease. EMBO J. *26*, 3144–3156. https://doi.org/10.1038/sj.emboj.7601745.

74. Vorontsova, O.V., Egorova, N.S., Arseniev, A.S., and Feofanov, A.V. (2011). Haemolytic and cytotoxic action of latarcin Ltc2a. Biochimie *93*, 227–241. https://doi.org/10.1016/j.biochi.2010.09.016.

75. Polyansky, A.A., Vassilevski, A.A., Volynsky, P.E., Vorontsova, O.V., Samsonova, O.V., Egorova, N.S., Krylov, N.A., Feofanov, A.V., Arseniev, A.S., Grishin, E.V., and Efremov, R.G. (2009). N-terminal amphipathic helix as a trigger of hemolytic activity in antimicrobial peptides: a case study in latarcins. FEBS Lett.

583, 2425–2428. https://doi.org/10.1016/j.febslet.2009.06.044.

76. Hawkins, C.J., Yoo, S.J., Peterson, E.P., Wang, S.L., Vernooy, S.Y., and Hay, B.A. (2000). The Drosophila caspase DRONC cleaves following glutamate or aspartate and is regulated by DIAP1, HID, and GRIM. J. Biol. Chem. *275*, 27084–27093. https://doi.org/10.1074/jbc.M000869200.

77. Shinoda, N., Hanawa, N., Chihara, T., Koto, A., and Miura, M. (2019). Dronc-independent basal executioner caspase activity sustains Drosophila imaginal tissue growth. Proc. Natl. Acad. Sci. USA *116*, 20539–20544. https://doi.org/10.1073/pnas.1904647116.

78. Song, Z., Guan, B., Bergman, A., Nicholson, D.W., Thornberry, N.A., Peterson, E.P., and Steller, H. (2000). Biochemical and genetic interactions between Drosophila caspases and the proapoptotic genes rpr, hid, and grim. Mol. Cell Biol. *20*, 2907–2914. https://doi.org/10.1128/MCB.20.8.2907-2914.2000.

79. Fraser, A.G., McCarthy, N.J., and Evan, G.I. (1997). drICE is an essential caspase required for apoptotic activity in Drosophila cells. EMBO J. *16*, 6192–6199. https://doi.org/10.1093/EMBOJ/16.20.6192.

80. Schanda, P., Kupĉe, E., and Brutscher, B. (2005). SOFAST-HMQC experiments for recording two-dimensional deteronuclear correlation spectra of proteins within a few seconds. J. Biomol. NMR *33*, 199–211. https://doi.org/10.1007/s10858-005-4425-x.

81. Vranken, W.F., Boucher, W., Stevens, T.J., Fogh, R.H., Pajon, A., Llinas, M., Ulrich, E.L., Markley, J.L., Ionides, J., and Laue, E.D. (2005). The CCPN data model for NMR spectroscopy: development of a software pipeline. Proteins *59*, 687–696. https://doi.org/10.1002/prot.20449.

82. Brunger, A.T. (2007). Version 1.2 of the crystallography and nmr system. Nat. Protoc. *2*, 2728–2733. https://doi.org/10.1038/nprot.2007.406.

83. Brünger, A.T., Adams, P.D., Clore, G.M., Delano, W.L., Gros, P., Grossekunstleve, R.W., Jiang, J.S., Kuszewski, J., Nilges, M., Pannu, N.S., et al. (1998). Crystallography & NMR system: a new software suite for macromolecular structure determination. Acta Crystallogr. D Biol. Crystallogr. *54*, 905–921. https://doi.org/10.1107/S0907444998003254.

84. Rieping, W., Habeck, M., Bardiaux, B., Bernard, A., Malliavin, T.E., and Nilges, M. (2007). ARIA2: automated NOE assignment and data integration in NMR structure calculation. Bioinformatics *23*, 381–382. https://doi.org/10.1093/bioinformatics/btl589.

85. Cheung, M.S., Maguire, M.L., Stevens, T.J., and Broadhurst, R.W. (2010). DANGLE: a Bayesian inferential method for predicting protein backbone dihedral angles and secondary structure. J. Magn. Reson. *202*, 223–233. https://doi.org/10.1016/j.jmr.2009.11.008.

86. Laskowski, R.A., Rullmannn, J.A., MacArthur, M.W., Kaptein, R., and Thornton, J.M. (1996). AQUA and PROCHECK-NMR: programs for checking the quality of protein structures solved by NMR. J. Biomol. NMR *8*, 477–486. https://doi.org/10.1007/BF00228148.

87. Hutchinson, E.G., and Thornton, J.M. (1996). Promotif - a program to identify and analyze structural motifs in proteins. Protein Sci. *5*, 212–220. https://doi.org/10.1002/pro.5560050204.

88. Pettersen, E.F., Goddard, T.D., Huang, C.C., Meng, E.C., Couch, G.S., Croll, T.I., Morris, J.H., and Ferrin, T.E. (2021). UCSF ChimeraX: structure visualization for researchers, educators, and developers. Protein Sci. *30*, 70–82. https://doi.org/10.1002/pro.3943.

89. DeLano, W.L. (2002). The PyMOL Molecular Graphics System (Delano Scientific).

STAR★METHODS

KEY RESOURCES TABLE

REAGENT or RESOURCE	SOURCE	IDENTIFIER
Antibodies		
Goat anti-rabbit secondary antibody, TexasRed	Thermo Fisher™	N/A
Rabbit Anti-U9 primary antibody	Eurogentec	N/A
Chemicals, peptides, and recombinant proteins		
M-Tb1a	PRIMACEN[33]	N/A
U9	Genscript	N/A
Z-VAD-FMK	AAT Bioquest	13300
7-Aminoactinomycin D	Invitrogen™	00-6993-50
Cycloheximide	Sigma-Aldrich	46401
Paraformaldehyde	Acros Organics	416785000
BSA	Sigma-Aldrich	A9647
Critical commercial assays		
CCK-8 assay	Boster Bio	AR1160
LDH assay	Interchim	CK12-05
CellEvent™ assay	Invitrogen™	C10723
ActinGreen™ 488 ReadyProbes™	Invitrogen™	R37110
ProLong™ Diamond Antifade Mountant with DAPI	Invitrogen™	P36966
Deposited data		
M-Tb1a 3D-structure	This study	BMRB Accession Code: 21100
U9 3D-Structure	This study	BMRB Accession Code: 21101
Lt2a 3D-structure	PDB[60]	Uniprot ID: Q1ELU1; PDB ID: 2G9P
Dk5a Sequence	Jensen et al., 2021[25]	N/A
Experimental models: Cell lines		
Drosophila S2 cells	Gibco™	R69007
Experimental models: Organisms/strains		
Blowflies (*L. caesar*)	Euroloisirs 81	N/A
Software and algorithms		
Las X v3.5.7.23225	Leica Microsystems	https://www.leica-microsystems.com/fr/
Brucker TopSpin	Brucker	https://www.bruker.com/fr.html
CCPNMR v2.2.2	CCPN	https://ccpn.ac.uk/
ARIA2 v2.3	Aria	http://aria.pasteur.fr/
Gen5 v3.10.06	Biotek	https://www.biotek.com/
ImageJ v1.53e	Imaje J	https://imagej.net/ij/index.html
GraphPad Prism v6.05	GraphPad	https://www.graphpad.com/

RESOURCE AVAILABILITY

Lead contact

Further information and requests for resources and reagents should be directed to and will be fulfilled by the lead contact, Elsa Bonnafé (elsa.bonnafe@univ-jfc.fr)

Materials availability

This study did not generate new unique reagents.

Data and code availability

NMR 3D-structures of M-Tb1a and U_9 have been deposited at Biological Magnetic Resonance Bank (BMRB) and are publicly available as of the date of publication. Accession numbers are listed in the key resources table.

This paper analyzes existing, publicly available data. These accession numbers or papers for the datasets are listed in the key resources table.

Any additional information required to reanalyze the data reported in this paper is available from the lead contact upon request.

EXPERIMENTAL MODEL AND SUBJECT DETAILS

Insect

L. caesar maggots were bought at Euroloisirs 81 and housed in a plastic box with a diameter of 100 mm. Maggots were kept at room temperature (25°C) until eclosion. Blowflies 1–4 days post-eclosion were used for insecticidal activity assays.

Insect cell line

The *Drosophila* S2 embryonic cell line (Thermofisher, USA) was maintained in Schneider's insect medium (Sigma-Aldrich, USA) supplemented with 10% heat-inactivated fetal bovine serum (Sigma-Aldrich) and 1% penicillin/streptomycin (Sigma-Aldrich) at 25°C without CO_2 on Tissue Cultured (TC)-treated support (Corning, USA). Cells were passaged every other days when they reached 90% confluence. For the experiments, cells were seeded at a density of 6.10^5 cells/mL, except for the CCK-8 assays, which were conducted at a cell density of 2.10^5 cells/mL.

METHOD DETAILS

Peptides

U_9 (GIVTKLIKKGVKLGLKMAL-$_{NH2}$) was chemically synthetized by GenScript® (Netherlands) with 95% purity. M-MYRTX-Tb1a (KIKIPWGKVKDFLVGGMKAV-$_{NH2}$) was synthesized as previously described[33] with a degree of purity higher than 99%. Peptides were solubilized at 2.2 mM in ultra-pure water (UPW) and stored at −40°C until use.

In vivo insecticidal assays

The insecticidal activity of U_9 and M-Tb1a was evaluated by intrathoracic injection of peptide dissolved in UPW at several concentrations and injected into blowflies (*Lucilia caesar*). A 1.0 mL Hamilton Syringe (1000 Series Gastight, Hamilton Company, NV, USA) with a fixed 25-G needle was attached to an Arnold hand microapplicator (Burkard Manufacturing Co. Ltd., England). Each fly received 1 μL of peptide solution and was individually housed in a 2-mL tube. Paralytic activity was assessed 1 h after injection. For each toxicity test and for the appropriate control (UPW solution; n = 10 flies), the test was repeated three times. Dose−response data were analyzed as detailed by Touchard et al.[14]

Cytotoxicity assays

CCK-8 (BosterBio, USA) and LDH (Interchim, France) assay kits were used to determine cell viability and mortality, respectively. Briefly, 100 μL of S2 cells at appropriate densities were seeded into TC-treated 96-well plates and incubated for 24hat 25°C. For the blanks, only culture medium was added in wells. Then, peptides were added at various concentrations (from 0.1 μM to 100 μM) for 24hat 25°C. Lysis Buffer and culture medium were used as positive (PC) and negative (NC) controls or blanks, respectively. In addition, the non-specific caspase inhibitor zVAD (AAT Bioquest, USA) at 100 μM in combination with the peptides was used to determine the involvement of caspases in peptide activity. The assays and calculations were performed following the manufacturer's instructions: CCK-8 was incubated with cells for 2 h and stirred for 10 min before reading absorbance at 450 nm and 490 nm for CCK-8 and LDH, respectively.

The relative percent mortality (LDH) or viability (CCK-8) was calculated according to the following equations using absorbance without blanks:

$$\text{Mortality}(\%) = \frac{\text{Peptide} - \text{NC}}{\text{PC} - \text{NC}} * 100 \quad \text{Viability}(\%) = \frac{\text{Peptide}}{\text{NC}} * 100$$

The LC_{50} of each peptide was determined by using the sigmoid equation in GraphPad Prism 6 software:

$$LC_{50} = \frac{\text{Bottom} + (\text{Top} - \text{Bottom})}{\left(1 + 10^{\left((\text{LogLC50} - X) * \text{HillSlope}\right)}\right)}$$

Membrane permeabilization assay

S2 cells were suspended and counted using trypan blue dye exclusion, then seeded in 96-well plates and incubated for 24hat 25°C. Then, cells were washed once with Phosphate Buffer Saline (PBS) 1X Ca^{2+}/Mg^{2+}, and once with culture medium before adding the peptides at the final concentrations (i.e., 50 μM for the high concentration, LC_{50} depending on the peptide and 3.33 μM for the sublytic concentration) diluted in the culture medium with 7-AAD (1:20). Fluorescence was recorded immediately using the TexasRed filter (λ_{ex}: 586/15 nm, λ_{em}: 647/57 nm). The fluorescent background of the images was removed before determining the ratio F_0/F. Curve fit was determined using linear regression for M-Tb1a and non-linear regression equations (quadratic model) for U_9.

Preparation of cell samples for SEM and TEM observations

S2 cells were seeded and incubated at 25°C for 24h on round glass coverslips sterilized with 70% ethanol, dried and placed in a TC-treated 24-well plate. Peptides were added to S2 cells at final concentrations (i.e., 50 μM for high concentration, LC_{50} depending on the peptide and 3.33 μM for sublytic concentration) and incubated at 25°C from 30 minutes to 24h. Untreated cells were used as controls. Fixation of samples was performed by adding 2% glutaraldehyde in 0.1 M Sorensen buffer (pH 7.4) at 4°C overnight.

Subsequent sample preparation was performed by CMEAB (TRI-GenoToul plateform, Toulouse, France): for TEM, fixed cells were washed twice in 0.2 M Sorensen Buffer (pH 7.4) for 12hat 4°C, then post-fixed for 1hat room temperature with 1% osmium tetroxide in 250 mM glucose and 0.5 M Sorensen buffer (pH 7.4). Samples were then dehydrated in a series of graded ethanol solutions, followed by acetone, and embedded in Epon resin (Embed 812, Electron Microscopy Sciences). Finally, cells were sliced into 70-nm thick sections (Reichert Jung Ultracut) and mounted on 100-mesh copper grids before staining with 3% uranyl acetate in 50% ethanol and Reynold's lead citrate. Examinations were carried out on a Hitachi HT7700 transmission electron microscope at an accelerating voltage of 80 kV.

For SEM, fixed cells were washed three times with distilled water, then dehydrated in a series of graded ethanol solutions and dried by critical point drying with a Leica EM CPD 300. Samples were coated with 6 nm platinium on a Leica EM Med 020 before being examined on a FEI Quanta 250 FEG scanning electron microscope, at an accelerating voltage of 5 kV.

Monitoring of Caspase-3 homolog (Drice/Dcp-1)

Caspase activity was monitored using the CellEvent™ Caspase-3/7 Green Detection Reagent (Thermofisher, USA). Normally, this kit is used for mammalian caspases 3/7 and their cleavage sites. Several studies have shown that Drice and Dcp-1, the *Drosophila* caspase-3 homologs, have the same cleavage site.[76–79] Consistent with these studies, the CellEvent™ kit was used on S2 cells to measure caspase-3 homologs (Dcp-1 and Drice). Cells were seeded in a TC-treated 96-well plate and incubated at 25°C for 24h. The culture medium was replaced with 100 μL of 4 μM CellEvent™ diluted in culture medium. The cells were then incubated with the peptides at final concentrations ranging from 0.1 to 50μM at 25°C for 24h. CHX (10 μM) and culture medium were used as positive and negative controls, respectively. Fluorescence was recorded using FITC filter (λ_{ex}: 469/35nm, λ_{em}: 525/39 nm) and the mean fluorescence intensity was determined from the unmodified images.

Immunocytochemistry

Glass coverslips were washed overnight with a methanol:chloroform (1:1) solution at room temperature (RT), sterilized with 70% ethanol, dried and placed in a 24-well plate. The coverslips were precoated with FBS for 2h at 37°C then washed twice with PBS 1X. S2 cells were seeded on the coverslips. They were then incubated at room temperature for 1.5 hours to let them adhere to the coverslips. Cells were treated with peptides at final concentrations (*i.e.* 50 μM for high concentration, LC_{50} depending on the peptide and 3.33 μM for sublytic concentration)for various exposure times ranging from 30 min to 24 h. Untreated cells were used as controls. Then, the cells were washed with PBS 1X and fixed with 4% paraformaldehyde at RT for 10 min. After permeabilization in PBST (PBS 1X + 0.1% Triton X-100) for 5 min (three times), the non-specific sites were blocked with 5% Bovine Serum Albumin (BSA) solution at RT for 1h. Cells were incubated overnight with 1:50 primary anti-U_9 antibody (EuroGentec, Belgium) in PBST solution with 1% BSA at 4°C. From this step on, incubations were performed at RT in the dark. The previous steps (from permeabilization in PBST to overnight incubation) were also performed by replacing PBTS with PBS to have non-permeabilized cells. Then, cells were washed three times in PBST for 5 min and stained for 1h with 1:500 secondary antibody labeled with TexasRed fluorochrome (Invitrogen™). Cells were washed twice with PBST and once with PBS 1X and stained with ActinGreen™ 488 ReadyProbes™ (AlexaFluor™ 488 phalloidin) Reagent (ThermoFisher), for 30 min. After two washes in PBS 1X, coverslips were mounted on a slide with ProLong™ Diamond Antifade Mountant with DAPI (Invitrogen™) and cured for 24h. Cells were visualized using a LEICA TCS SP8 AOBS confocal microscope through a HC PL APO 63x/1.40 CS2 oil immersion objective with the following lasers: 405 nm for DAPI (5% intensity), 488 nm for FITC (2% intensity) and 561 nm for TexasRed (5% intensity). Images were acquired using LAS X software (v3.5.7.23225) with the z-Stack tool and analyzed after z-Stack projection to obtain 2D and 3D images.

NMR experiments

Each synthesized peptide was dissolved in 50% 2,2,2-trifluoroethanol-d2 at a concentration of 0.8 mM for U_9 and 1.2 mM for M-Tb1a. Then, 2D 1H-NOESY (150 ms mixing time), 2D 1H-TOCSY (80 ms mixing time), sofast-HMQC[80] (^{15}N natural abundance) and ^{13}C HSQC (^{13}C natural abundance) spectra were performed at 298K on a BRUKER 700 MHz Avance III HD spectrometer equipped with a cryoprobe. ^{1}H chemical shifts were referenced to the water signal (4.77ppmat 298K). NMR data were processed using the Bruker TopSpin software version 3.6.2^{TM} and analyzed with CCPNMR version 2.2.2.[81] Analysis of the 2D-TOCSY and NOESY spectra allowed for a complete assignment of ^{1}H chemical shifts using natural-abundance heteronuclear NMR spectra.

Structure calculations

Structures were calculated using the Cristallography and NMR System (CNS)[82,83] through the automatic assignment software ARIA2 version 2.3[84] with NOE-derived distances, hydrogen bonds (consistent with the observation of a typical distance NOE cross-peak network for the α-helix) and backbone dihedral angle restraints determined with the DANGLE program[85] only for U_9. The ARIA2 protocol, with default parameters used simulated annealing with torsion angle and Cartesian space dynamics. The iterative process was repeated until the NOE cross-peak assignment was complete. The final run for each peptide was performed with 1000 initial structures, and 250 structures were refined in water. 15 structures were selected based on total energies and restraint violation statistics to represent the three dimensional structures of the U_9 and M-Tb1a peptides in solution. The quality of the final structures was evaluated using PROCHECK-NMR[86] and PROMOTIF.[87]

Structure calculations were performed without considering C-ter amidation in particular because no NOE could be observed between the C-ter amido protons (Val20-NH2 for M-Tb1a and Leu19-NH2 for U_9) and all other protons in each peptide. However, the Coulombic electrostatic potential (ESP) and Molecular lipophilicity potential (MLP) were determined at the Connoly surface of the peptide after C-ter amidation using ChimeraX 1.3.[88] Figures were prepared with PYMOL[89] and ChimeraX.

NMR data and three dimensional structure coordinates have been deposited with SMSDep under the Biological Magnetic Resonance Bank (BMRB) accession codes: 21100 (M-Tb1a) and 21101 (U_9).

QUANTIFICATION AND STATISTICAL ANALYSIS

Data and statistical analysis

Images (except for SEM, TEM, and immunocytochemistry experiments), absorbance and fluorescence data were acquired with the Biotek Cytation 1 microplate reader (Agilent Technologies, USA) using Gen5 software (Biotek, v3.10.06). Images were analyzed using ImageJ (1.53e) or Gen5 software (Biotek, v3.10.06). Graphs and statistics were prepared and analyzed using GraphPad Prism 6 software (v6.05). Normal distribution of data was determined by the Shapiro-Wilk test and homogeneity of variances by the Fisher test. If the data do not follow a normal distribution and/or do not have a homogeneous variance, a non-parametric test was performed. The statistical details and the replicate number of experiments can be found in the figure legends.